NASA CONTRACTOR
REPORT

NASA CR-178996

A CRITICAL EVALUATION OF VARIOUS METHODS FOR THE ANALYSIS
OF FLOW-SOLID INTERACTION IN A NEST OF THIN CYLINDERS
SUBJECTED TO CROSS FLOWS

By Sang-Wook Kim
Universities Space Research Association
Systems Dynamics Laboratory
Science and Engineering Directorate

Interim Report

January 1987

ACKNOWLEDGMENTS

TABLE OF CONTENTS

LIST OF ILLUSTRATIONS

LIST OF TABLES

$\dot{a}$ time rate of change of $\underset{\sim}{a}$

$\underset{\approx}{B}$ a matrix relating strain vector to nodal displacements, $\underset{\approx}{B} = \underset{\approx}{L}\underset{\approx}{N}$

$\underset{\sim}{b}$ body force vector (includes acceleration force)

C_a inertia coefficient for displaced fluid due to vibration of structure

c_Δ a coefficient used in LES subgrid-scale model

$\underset{\approx}{\hat{D}}^n$ elasto-viscoplastic material property matrix

d diameter of a cylinder

E Young's modulus

F yield function

$\underset{\sim}{f}$ load vector in a system of equations

f_b dominant frequency of turbulent buffeting spectrum

f_n natural frequency of a cylinder

f_{vs} vortex shedding frequency

$G(\underset{\sim}{x}, \underset{\sim}{x}')$ filtering function for LES method

I area moment of inertia

$\underset{\sim}{I}$ identity matrix

$\underset{\sim}{K}$ finite element stiffness matrix

K_{fe} an experimentally determined constant for fluidelastic instability equation

$\underset{\approx}{K}^n_T$ tangential stiffness matrix for elasto-viscoplastic finite element equation

$\underset{\approx}{k}_0''$ artificial viscosity in Petrov-Galerkin finite element method

$\underset{\approx}{L}$ differential operator relating strain to displacement

l length scale of energy containing eddies

$\underset{\approx}{M}$ mass matrix

m added mass, $m = m_0 + C_a \pi \rho d^2 / 4$

m_0 mass per unit length of a cylinder

$\underset{\sim}{N}$ matrix of interpolating polynomials

N_e	number of nodes in an element
P_e	Peclet number
p_m	mode shape function for sound pressure
p_s	sound pressure
Re_d	Reynolds number, $\rho U d / \mu$
R_t	turbulent Reynolds number
S_b	Strouhal number based on dominant frequency of turbulent buffeting spectrum
S_1	cylinder spacing in flow direction in a tube bank
S_t	cylinder spacing in normal to the flow direction in a tube bank
S_{vs}	Strouhal number based on vortex shedding frequency
$\underset{\sim}{u}$	displacement vector in spatial coordinate directions
V	free stream flow velocity
V_g	flow velocity between cylinders in a nest of cylinders
v	velocity vector in spatial coordinate direction
α	a constant coefficient used in fluidelastic instability equation
α_p	penalty parameter for penalty finite element method
β	a constant coefficient used in fluidelastic instability equation
γ	a constant coefficient used in fluidelastic instability equation
γ_p	fluidity of plastic flows
Δ	twice of the computational mesh size in LES method
Δt^n	time increment, $\Delta t^n = t^{n+1} - t^n$
δ	dimensionless logarithmic decrement of amplitude due to fluid and structural damping
δ_{ij}	Kronecker delta (=1 for i = j, = 0 for i ≠ j)
$\delta \underset{\sim}{u}$	variation of displacements
ε	turbulent dissipation function
$\underset{\sim}{\varepsilon}$	a column vector of strain (or total strain)
$\underset{\sim}{\varepsilon}_e$	a column vector of elastic strain

$\underset{\sim}{\varepsilon}_{vp}$	a column vector of viscoplastic strain
Θ	interpolation parameter
μ	molecular viscosity of a fluid
ν_t	eddy viscosity
π	a constant, $\pi = 3.141592654$
ρ	fluid density
ω	radian frequency
$\underset{\sim}{\omega}$	vorticity vector
$\partial\Omega$	boundary of domain
$\partial\Omega_1$	part of boundary on which Dirichlet boundary condition is specified
$\partial\Omega_2$	part of boundary on which Neumann boundary condition is specified
$\phi_k(x)$	finite element basis polynomial, $k = 1, N_e$

CONTRACT REPORT

A CRITICAL EVALUATION OF VARIOUS METHODS FOR THE ANALYSIS OF
FLOW-SOLID INTERACTION IN A NEST OF THIN CYLINDERS
SUBJECTED TO CROSS FLOWS

I. INTRODUCTION

Cross flows over a cylinder or a nest of cylinders can be found in chimney stacks, aircrafts and missiles at high angles of attack, marine tow cables, offshore oil rigs and platforms, heat exchanger tube banks, and in the Space Shuttle Main Engine. These flows induce the structures to vibrate and the vibrating structures alter the flow field so that the fluid and the structural motions are strongly coupled together. It is imperative to understand the flow induced vibrations and to have predictive ability to avoid failure of structures. This report contains a critical evaluation of various methods of analysis for flow induced vibrations of a nest of cylinders in cross flows as well as a critical evaluation of existing numerical methods for flow-solid interactions.

Topics included in Section 2 are: description of discrete vibration inducing mechanisms for a nest of cylinders; experimental correlation equations derived through physical arguments or analytical modelings; recent developments in semi-numerical modeling of the flow-induced vibrations due to multiple number of vibration inducing mechanisms; and accumulated experimental data which are used as design guides for tube banks.

Flow-solid interactions have been studied for the last two decades. Nevertheless, application of major numerical analysis methods such as the finite difference method and the finite element method to these problems is still in its early development stage, and there exists only a limited number of publications related to these topics. In-depth prediction methods to be developed in the future for flow-solid interactions of a nest of cylinders in a cross flow, a problem which is geometrically and materially nonlinear in nature, would require major improvements in numerical analysis methods, unsteady turbulence models, and structural analysis methods including large and/or permanent deformations. Recent developments on these topics are discussed in Section 3.

In addition to reviewing the flow-solid interaction analysis methods for tube banks, most recently available experimental data as well as experimental correlation equations are included in this report in order to provide a stand-alone guideline for design of tube banks. Also some of the finite element methods for flows as well as for structures, which may be used advantageously in the future development of a numerical analysis method for flow-solid interaction of tube banks, are discussed in some detail.

II. CROSS FLOW INDUCED VIBRATIONS

Vibration of a cylinder or a nest of cylinders in cross flows is induced by vortex shedding, fluctuating turbulent wall pressure (buffeting), fluidelastic coupling, jet switching, oscillating mean free stream flows, and aerodynamic noise generated in

the flow field. In many practical cases, all of the vibration generating mechanisms act synergistically rather than separately. Consequently, detailed analytical modeling of the fully coupled flow-solid interaction is difficult. But depending on the arrangement of cylinders, flow velocities, and Reynolds numbers, a few of the vibration generating mechanisms usually dominate the rest so that rather simple analytical models can be developed. Most of the available analytical models are for these simple flow-solid interaction cases; yet these are also important tools in preliminary design analysis of tube banks. For practical design of tube banks, the experimental correlation equations, obtained by curve-fitting of experimental data, are used as design criteria. Each of the above vibration generating mechanisms, analytical models, experimental correlation equations, experimental data, and semi-numerical solutions are discussed below.

2.1 Vortex Induced Vibration

In the frontal area of a cylinder, boundary layers are formed on the top and bottom surfaces of the cylinder. As the fluid particles in the boundary layers travel toward the rear end, the linear momentum of fluid particles is dissipated in overcoming the adverse pressure gradient in the rear part of the cylinder. When the momentum is completely lost, the boundary layers separate and form two free shear layers which bound the wake. Since the fluid particles near the center line travel much slower than those near the free stream, these shear layers roll up into discrete vortices. The pattern of vortex shedding for a rigid cylinder changes as the Reynolds number, Re_d, is changed [1]. Discrete laminar vortices begin to appear at approximately $Re_d = 40$. The vortex flow becomes turbulent at Re_d as low as 150; the boundary layer flows become turbulent for $Re_d \geq 3 \times 10^5$; the turbulent wake becomes narrower and disorganized up to $Re_d = 3.5 \times 10^6$; and organized turbulent vortex street is formed again for Re_d higher than 3.5×10^6.

For flow-solid interaction occurring when a cylinder is subjected to cross flow, only at low Reynolds numbers, vortex shedding is the major source of mechanical excitation. As soon as turbulence begins to appear in the flow field or if the free stream is turbulent (i.e., beginning from turbulence intensities 2 to 4 percent), the fluctuating turbulent wall pressure (buffeting) becomes a source of mechanical excitation which is of equal importance as the vortex shedding. As the free stream flow velocity is increased or decreased so that the vortex shedding frequency approaches the natural frequency of the cylinder, resonant vibration with large amplitude is produced.

For a single row of cylinders placed perpendicular to the flow direction, vortex shedding is the major source of mechanical excitation only for small values of $V_g/f_n d$, where V_g is the flow velocity between the cylinders and f_n is the natural frequency of a cylinder. As soon as $V_g/f_n d$ is increased, fluctuating turbulent wall pressure becomes an equally important source of excitation as the vortex shedding; and for $V_g/f_n d > 75$, jet switching dominates the rest of vibration inducing mechanisms [3,4].

Cylinders in a closely spaced tube bank do not respond as single cylinders; rather, interaction with the flow field causes coupled motion in the group of cylinders. The vortex shedding is confined to a range of moderate to large cylinder spacing ratios in tube banks [2]. For $S_t/d < 1.5$, vortex shedding would be suppressed due

2

to proximity to the cylinders [1], where S_t is the cylinder spacing in normal to the flow direction as shown in Figure 1. Idealized response of a cylinder in a nest of cylinders (tube bank) to increasing flow velocity is shown in Figure 2 [5]. It can be seen in Figure 2 that the resonance to fluid periodicity, i.e., resonance to fluctuating turbulent wall pressure or vortex shedding, and fluidelastic instability are the most important mechanisms that can cause failure of tube banks.
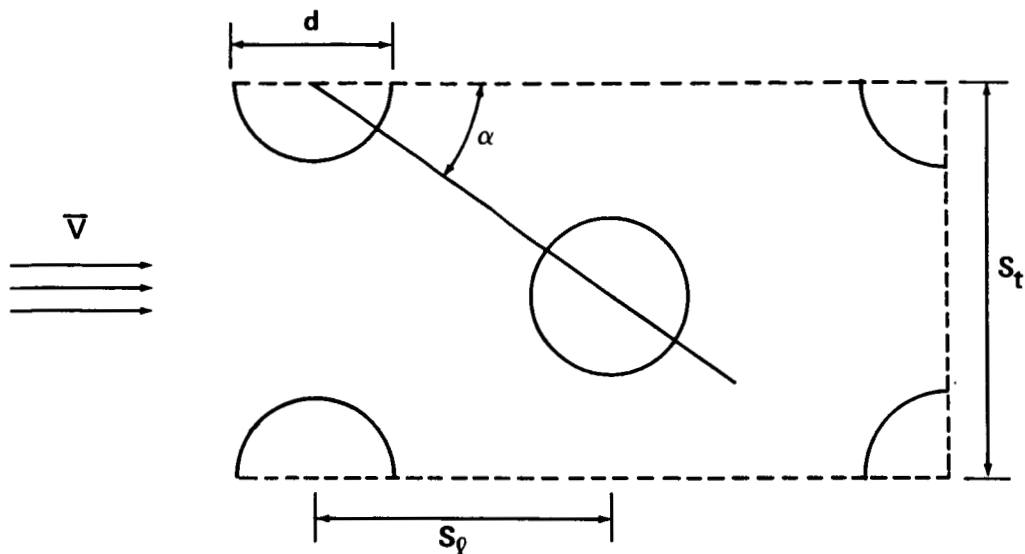
Figure 1. Parameters used for a nest of cylinders.
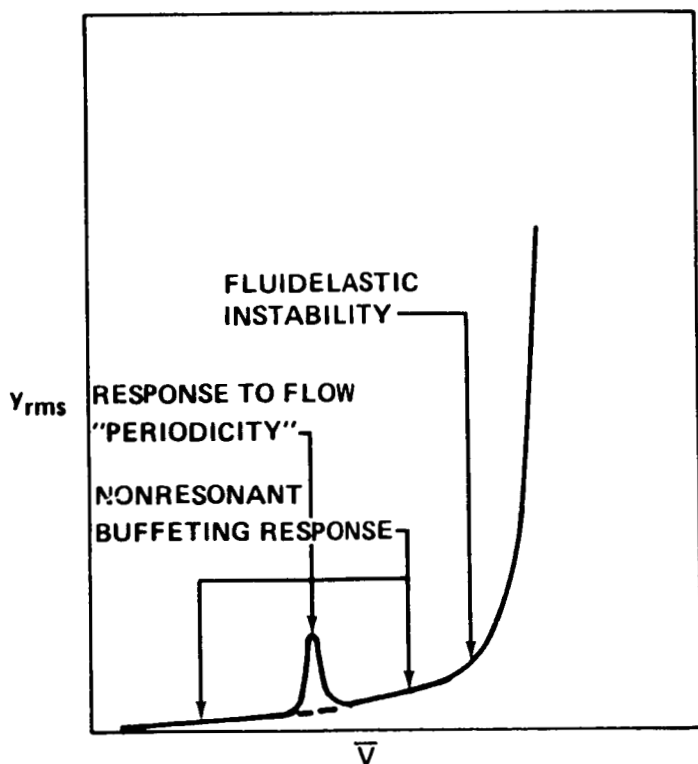
Figure 2. Idealized response of a cylinder in a nest of cylinders subjected to cross flow.

3

Vibrations due to vortex shedding and buffeting are classified as forced vibrations since these two vibration inducing mechanisms do not require flow-solid interactions and can exist for flow around rigid bodies. The experimental correlation equations, used by tube bank designers to avoid resonance to vortex shedding, are usually developed on the basis of the contribution of Chen [6]. On the other hand, correlation equations developed on the basis of the theory formulated by Owen [7] provide design means to avoid resonance to fluctuating turbulent wall pressure (buffeting). Later, Paidoussis [8] showed that the two seemingly different conditions for resonance represent the same physical phenomenon and the only difference depends on the physical interpretation of the mechanism that induces resonance. In fact, as shown in Figure 2, the vibration due to vortex shedding, if it exists, and buffeting coexist in the low free stream velocity region.

The correlation equation derived by Chen [6], for resonance in vortex induced vibration, is given as:

$$f_n d / V_g = S_{vs} \quad , \tag{2.1}$$

where $S_{vs} = f_{vs} d / V_g$ is the Strouhal number, f_{vs} is the vortex shedding frequency, and the rest of the notations are the same as before. A table of S_{vs} for various geometrical arrangement of cylinders can be found in Reference 6. Resonance to vortex shedding can be avoided by rendering the left hand side of equation (2.1) to be different, by 40 to 50 percent, from the Strouhal number which will cause resonance for a particular arrangement of cylinders.

2.2 Fluctuating Turbulent Wall Pressure

Turbulent flows induce vibration of structures through the fluctuating turbulent wall pressure acting on the surface of structures submerged in the flow field.

A nest of cylinders subjected to cross flow exhibit a peak amplitude at a flow speed whose dominant frequency of fluctuating turbulent wall pressure spectrum coincides with the natural frequency of the submerged cylinders. Most of the experimental correlation equations used for predicting resonance which is caused by buffeting are based on the expression developed by Owen [7].

The correlation equation due to Owen [7] is based on the assumptions that: the conditions for fully turbulent flow have been developed through regions sufficiently deep inside the tube bank; the rates of production and dissipation of the turbulent kinetic energy are in equilibrium; the length scale of the energy containing eddies is of the same order of magnitude as the cylinder spacing in the flow direction; the source of vibration is associated with the randomly fluctuating pressure forces imposed on the cylinders by the turbulent eddies; the flow velocity is low enough so that the fluidelastic vibration would not occur, yet the Reynolds number is high enough so that the effect of molecular viscosity is negligible; the tube spacing normal to the flow direction, S_t/d, is appreciably greater than unity so that a cylinder preserves some of the features of a circular cylinder in isolation but not large enough for these features to dominate; and the rate of dissipation of turbulent energy and the work done by the mean pressure gradient across any row of cylinders are in balance as has

4

been observed in experiments. The correlation equation due to Owen [7] states that buffeting resonance would occur if:

$$f_n d / V_g = S_b \quad , \tag{2.2}$$

where V_g is defined to be the flow velocity at the minimum gap in a row, $S_b = f_b d / V_g$ is a Strouhal number, f_b is the dominant frequency of the turbulent buffeting spectrum, and the rest of the notations are the same as before. According to Owen [7], f_b is given as:

$$f_b = \frac{V_g}{\ell} \frac{1}{(1 - d/S_t)} [3.05 (1 - \frac{d}{S_t})^2 + 0.28] \quad ,$$

where ℓ is the length scale of the energy containing eddies, and the rest of the notations are the same as before. It was mentioned that equations (2.1) and (2.2) represent the same phyiscal resonance conditions at low free stream velocities [5]. Nevertheless, there exists significant quantitative difference between these two equations if they are plotted on the same graph. Therefore, equations (2.1) and (2.2) can provide only rough criteria for avoiding resonance to forced vibration in the design of a tube bank.

A prediction method, which utilizes the random vibration theory [9,10] for the maximum amplitude in resonant forced vibration was developed by Chen and Wambsganss [11,12]. In this method, it is required to know the spectra and frequency composition of fluctuating turbulent wall pressure. For preliminary design analysis, neither the distribution of turbulent wall pressure as function of time nor the spectra and frequency composition are known a priori. Therefore, a set of data obtained from flat plate measurements have been used in References 11 and 12 to predict the maximum amplitude. The specific example problem in References 11 and 12 will not be discussed herein. General procedures for flow induced random vibration analysis can be found in References 9 and 10.

Recently, methods for predicting fluctuating turbulent wall pressures [13,14] and more detailed experimental data [15] have begun to appear in the open literature. Use of such a prediction method in a finite element analysis of compliant plates has been reported in References 16 and 17. These will be discussed in Section 3.2.

2.3 Fluidelastic Instability

Tube banks subjected to increasing flow velocity begin to vibrate with large amplitude at a critical flow velocity with a definite frequency or a group of frequencies which are different from that of the natural vibration mode of the cylinders. Above the critical flow velocity, the amplitude of vibration increases as the square of the flow velocity, apparently without limit. In this type of vibration, called fluidelastic or aeroelastic vibrations, the flow field excites the structure to vibrate and in turn the vibrating structure disturbs the fluctuation inducing flow field. Accordingly, this is a fully coupled flow-solid interaction phenomenon and is classified as a self-excited vibration.

Fluidelastic instability is of utmost concern in tube bank designs because it can cause total failure in the structural system. On the other hand, resonance to forced vibrations, i.e., vibrations due to vortex shedding and/or buffeting is of less concern, because it can be avoided by keeping the flow velocities away from the expected resonance velocity by a factor of 40 to 50 percent.

The analytical expression for the onset of fluidelastic instability for a row of cylinders placed perpendicular to the flow direction was first proposed by Connors [4], and is given as:

$$V_g/f_b d = K_{fe}(m\delta/\rho d^2)\alpha \quad , \tag{2.4}$$

where the gap velocity V_g is defined as $V_g = V[(S_t/d)/\{(S_t/d)-1\}]$; K_{fe} is a constant, or a function of cylinder spacing to be determined from experiments; α is a constant to be derived from theoretical analysis, yet it can be modified to fit experimental data more precisely; ρ is the density of the fluid; m is the added mass defined as $m = m_0 + C_a \pi \rho d^2/4$; m_0 is the mass per unit length of the cylinder; C_a is an experimentally determined inertia coefficient for displaced fluid due to structural vibration [1]; $\pi = 3.14159$; δ is the logarithmic decrement of amplitude due to fluid and structural damping which is dimensionless; and the rest of the notations are the same as before. Equation (2.4) was derived by assuming that the energy supplied to the structural vibration would be equal to the energy dissipated by the damping force to maintain equilibrium in fluidelastic vibration.

Following the line of Connors [4], Blevins [18] formulated an analytical model which is more rigorous mathematically. The underlying assumptions in his modeling are: the vortex shedding frequency of the cylinders is well above the natural frequency of the cylinders so that the cylinders are not excited by vortex shedding or buffeting; flow velocity is low enough so that jet switching is inactive; and the forces due to asymmetry of the flow pattern caused by the displacement of cylinders from equilibrium is the only source of vibration. Blevins [18] sub-divided the fluidelastic instability criterion into three cases depending on vibration frequencies and damping forces along and transverse to the flow direction. These are: a symmetric frequency and symmetric damping force case, an asymmetric frequency and asymmetric damping force case. The first case of Blevins [18] reproduced exactly the same result as that obtained by Connors [4]. Later, Heinecke [19] showed that the same equation, equation (2.4), can be derived by simple dimensional analysis and energy consideration of a dampled, hormonically excited oscillator. From the underlying assumptions of Blevin's [18] and Heinecke's [19] models, it might be suspected that the Connors' criterion for fluidelastic instability is not conservative. In fact, a list of failure cases of tube banks, which satisfied the Connors' fluidelastic instability criterion, can be found in Reference 8.

Numerous experimental correlation equations have been derived following the line of Connors' work by incorporating more experimental data into equation (2.4). In order to provide a stand-alone guideline for tube bank designs, different values of the coefficient K_{fe} and exponent α in equation (2.4), proposed by many different groups of workers in the area, are summarized in Table 1 [20].

TABLE 1. VALUES OF K_{fe} AND α [20]

Investigators	K_{fe}	α	Remarks
Connors [4]	9.9	0.5	Tube row with $S_t/d = 1.42$
Blevins [18]	$\dfrac{2(2\pi)^{0.5}}{(C_x C_y)^{0.25}}$	0.5	C_x and C_y are fluid-elastic-stiffness force coefficients
Y. N. Chen [21]	$\beta\, Re^{-0.25}$	0.5	Re = Reynolds number, β = constant
Gross [22]	4/k	1.0	For square array, and k determined from fluid force
Gorman [23]	3.3	0.5	Suggested design guideline
Savkar [24]	$4.95\,(S_t/d)^2$	0.5	For triangular arrays
Connors [25]	$0.37 + 1.76\, S_t/d$	0.5	For square array $1.41 \le S_t/d \le 2.12$
Pettigrew et al. [26]	3.3	0.5	Suggested design guideline
Weaver and Grover [27]	7.1	0.21	Rotated triangular array $S_t/d = 1.375$
Chen and Jendrzejczyk	2.49 to 6.03	0.2 to 1.08	For various rectangular arrays and mixed array in water flow
Tanaka et al. [29]	3.0	0.75	For square array, $S_t/d = 2.0$

Another type of empirical correlation equation has been developed by means of similitude analysis [27]. This equation is given as:

$$\frac{V_g}{f_n d} = B\left(\frac{m}{\rho d^2}\right)^2 \delta^\beta \left(\frac{S_t}{d} - 1\right)^\gamma \tag{2.5}$$

where α, β, and γ are exponents to be determined from experiments; B is a constant, or might be a function of other nondimensional parameters; the gap velocity, V_g, is defined in the same way as in equation (2.4); and the rest of the notations are

the same as before. The experimentally determined coefficients by many researchers are summarized in Table 2 [20].

TABLE 2. VALUES OF COEFFICIENTS FOR EQUATION (2.5) [20]

Investigators	B	α	β	γ	Remark (Based on published data)
Paidoussis [8]	2.3	0.5	0.25	1	Includes all data
Paidoussis [30]	5.8	0.4	0.4	1	Excludes some data

All these theories and data appearing in Tables 1 and 2 have been assembled and presented by Chen [20] for different tube patterns, i.e., according to different geometrical arrangements of cylinders. These are shown in Table 3. Blevins [31] pointed out, however, that any dependence of this data on tube pattern is masked by the data scatter and suggested to use a single least squares curve-fitted expression as shown in Figure 3 [31,32]. A similar single graphical representation of most of the experimental data that are available to date for fluidelastic instability prediction of triangular arrays of cylinders, has been compiled by Chen [33], and is given in Figure 4.

TABLE 3. LOWER BOUND ON CRITICAL FLOW VELOCITY [20]

Array	θ	Parameter Range for δ_m	$V_g/f_n d$
Tube row	-	$0.05 < \delta_m < 0.3$	$1.35 \, (S_t/d - 0.375) \delta_m^{0.06}$
		$0.3 \;\; < \delta_m < 4.0$	$2.30 \, (S_t/d - 0.375) \delta_m^{0.5}$
		$4.0 \;\; < \delta_m < 300$	$6.00 \, (S_t/d - 0.375) \delta_m^{0.5}$
Square	90°	$0.03 < \delta_m < 0.7$	$2.10 \delta_m^{0.15}$
		$0.7 \;\; < \delta_m < 300$	$2.35 \delta_m^{0.50}$
Rotated square	45°	$0.1 < \delta_m < 300$	$3.54 \, (S_t/d - 0.5) \delta_m^{0.5}$
Triangular	30°	$0.1 < \delta_m < 2$	$3.58 \, (S_t/d - 0.9) \delta_m^{0.1}$
		$2 \;\;\;\; < \delta_m < 300$	$6.53 \, (S_t/d - 0.9) \delta_m^{0.5}$
Rotated triangular	60°	$0.01 < \delta_m < 1$	$2.8 \delta_m^{0.17}$
		$1 \;\;\; < \delta_m < 300$	$2.8 \delta_m^{0.5}$

* θ is defined in Figure 1.

** $\delta_m = m\delta/\rho d^2$.

8
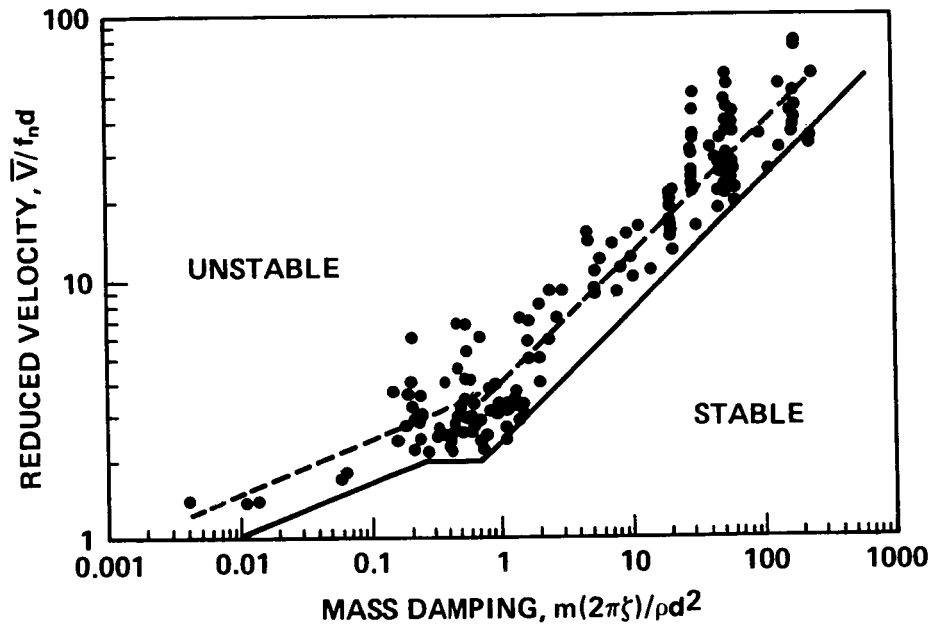
Figure 3. Mean and lower boundary curves for fluidelastic instability [31].
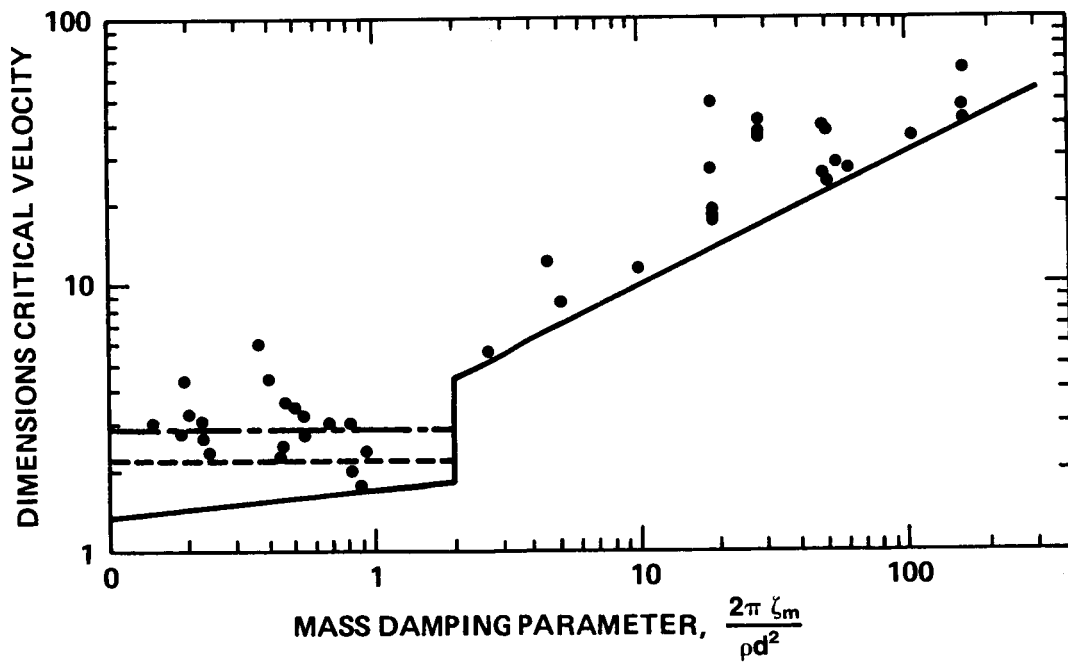
Figure 4. Stability diagram for triangular arrays of cylinders [33].

2.4 Other Vibration Inducing Mechanisms

Other vibration-inducing mechanisms are: (1) aeroacoustic noise; (2) swirling flows; and (3) oscillating mean free-stream velocity. These vibration sources have received less attention than the others considered earlier in this section, and are more difficult to treat, both analytically as well as experimentally, especially for tube banks. Another vibration inducing source is jet switching which is a type of fluid-elastic vibration and can be observed most prominently for a single row of cylinders subjected to cross flows. Jet switching is included in this section.

2.4.1 Aeroacoustic Noise

Aeroacoustic sound is generated by vortex shedding and turbulence. If the vortex shedding frequency coincides with the acoustic frequency, then the two mechanisms reinforce each other. Furthermore, if these two frequencies approach the natural frequency of cylinders, then large amplitude vibration which can lead to failure of tube banks can be caused.

A review of numerous analytical and finite difference numerical solution of acoustic wave propagation in both homogeneous and inhomogeneous medium can be found in Candel [34]. The acoustic wave propagation equations considered in Reference 34 are a direct wave propagation equation and the Helmholtz equation. The direct wave propagation equation is given as:

$$\frac{\partial^2 P_s}{\partial t^2} - c^2 \nabla^2 P_s = 0 \quad , \tag{2.6}$$

where P_s is the sound pressure, t is time, c is the speed of sound, $c = c(\underline{x})$, $\underline{x}$ is the spatial coordinates, and ∇^2 is the Laplacian operator. The Helmholtz equation can be obtained from equation (2.6) by setting

$$P_s = P_m e^{i\omega t} \quad , \tag{2.7}$$

where $p_m(x)$ is the mode shape function, e is the natural base of logarithm, $i = \sqrt{-1}$, and ω is the radian frequency. A finite element analysis of Helmholtz equation for optimal design of acoustic chamber can be found in Bernhard [35].

A review of sound induced by vortex shedding from cylinders is given by Blevins [36]. The governing equation considered in the review is the Lighthill's equation given as:

$$\frac{\partial^2 \rho}{\partial t^2} - c^2 \nabla^2 \rho = \frac{\partial^2}{\partial x_i \, \partial x_j} T_{ij} \quad , \tag{2.8}$$

10

where $T_{ij} = \rho v_i v_j - \tau_{ij} - c^2 p \delta_{ij}$, τ_{ij} is the fluid stress tensor, δ_{ij} is the Kronecker delta, and the rest of the notations are the same as before.

Recently, Quinn and Howe [37] presented an analytical solution for acoustic wave propagation through a tube bank. They modeled the cylinders as rigid finite flat plates at zero angle of attack. The effect of vortex shedding was incorporated in their equation by inserting aeroacoustic dipole sources in the forcing function term of the classical velocity potential equation for acoustic wave equation. The result of this analysis showed qualitatively that both attenuation and sound speed increase with decreasing frequency in such a way that onset of resonance is delayed.

Blevins [36] concluded that the degree to which self-sound synchronizes vortex shedding from various tubes is not known and that the role of acoustic damping had not been well understood until now.

More recently, an experimental study to eliminate aerodynamic noise in a tube bank was reported by Zdravkovich and Nuttall [38]. Experiments were performed with a tube bank of three rows of cylinders, with seven cylinders per each row. The array of cylinders is shown in Figure 5. It was shown that the acoustic resonance could be eliminated either by spacing unequally two successive rows of cylinders or by removing certain cylinders from the tube bank. Removal of a few cylinders from the first row was found to be the most effective way to eliminate acoustic resonance. For the second row, removal of a few cylinders was effective only at the pressure nodes; while removal in the third row was not effective at all.

Other approaches to reduce aeroacoustic noise was also found by Baird [39] and Cohan and Dean [40]. They recommended to use baffles in order to avoid the first and higher modes of standing waves, but this technique may not be used advantageously for densely populated cylinders because of high pressure drop in the tube bank [40].
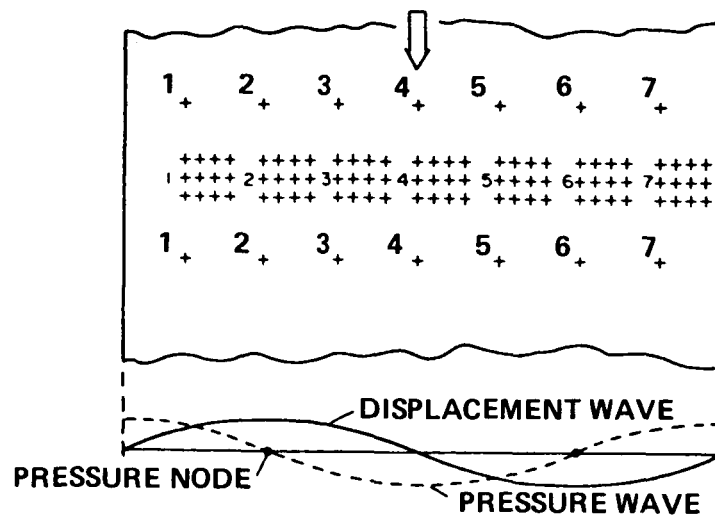
Figure 5. Possible tube arrangements to reduce aeroacoustic noise [37].

2.4.2 Jet Switching

In this phenomenon, fluid forces excite the cylinders to vibrate and the displacement of cylinders cause the jet pairs emerging from closely spaced cylinders to switch. Jet switching is a self-excited vibration which requires fully coupled flow-solid interaction. Coupling of jets in the wake region of a row of cylinders is shown in Figure 6.
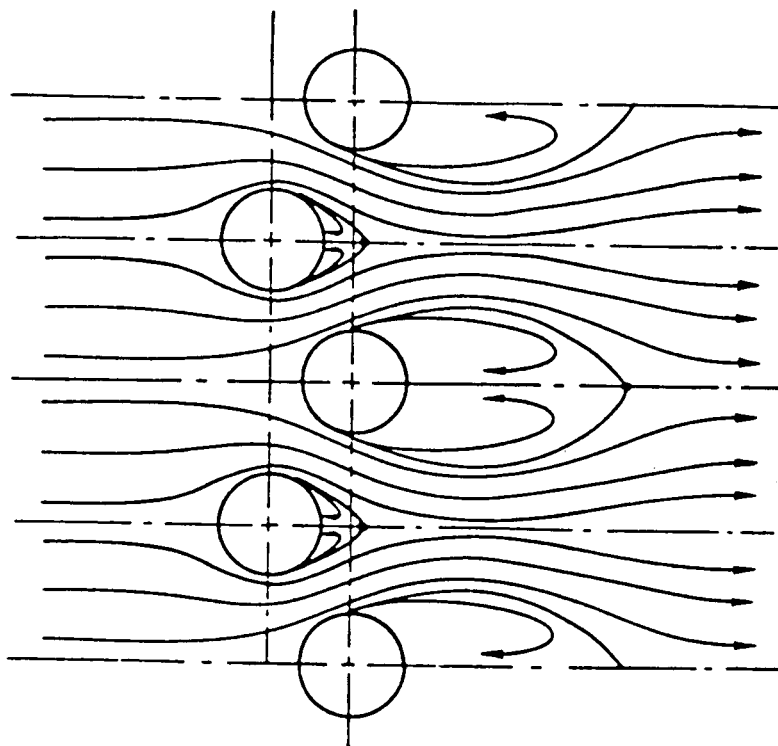
Figure 6.   Coupling of jets in the wake region of a row of cylinders subjected to cross-flow [1].

It was claimed in Reference 3 that jet switching may not occur for $V_g/f_n d < 75$, and it was reported in Reference 4 that jet switching was not observed for $V_g/f_n d < 30$.

It was observed experimentally that the flow slightly inside the tube bank is suppressed so that jet switching is confined to a few cylinders at the flow inlet region. The cylinders at the flow inlet region are subjected to the greatest fluid force as well as to jet switching. Consequently, these cylinders are most susceptible to damage due to fatigue and inelastic deformation due to large displacements. Closed form analytical solutions cannot take this fact into account. Also numerical analysis for this type of problem has not been attempted as yet. However, experimental correlation equations include this phenomenon implicitly, for experiments are concerned with failure of tube banks in an integrated sense.

2.4.3 Oscillating Mean Flows and Swirling Flows

Oscillating mean flows and swirling flows excite a nest of cylinders submerged in the flow field to vibrate. Analytical analysis of flow induced vibrations due to oscillating mean flows is mostly based on the approach proposed by Morison [41], in which a cylinder is represented by an Euler beam and the fluid force acting on the cylinder is modeled as forcing function in the Euler beam equation. Most of the recent analyses have concentrated on modeling the fluid force due to oscillating mean flow, but flow-solid interaction has seldom been considered.

It is natural to expect the swirling flows would induce vibration of cylinders submerged in the flow field. More importantly, the swirling component of the flow can alter the entire flow field so that the vibration mode of submerged cylinders may be different from those without swirl velocity. For example, it is well known that the flow field of jets with swirling component is quite different from those without swirling component [42]. Swirling flow through a nest of cylinders can be found in a swirl crossflow stirling engine heater [43] or in the Space Shuttle Main Engine (SSME) Main Injector Assembly (MIA) (Fig. 7). A finite difference numerical analysis of the flow field inside MIA showed that there exists the swirling flow [44] (Fig. 8). As a remark, the vibration of cylinders has not been considered in Reference 43 or 44. Only the heat transfer rate was considered experimentally in Reference 43. Neither the details of flow field inside tube banks nor the effect of swirl flow on vibration of cylinders are known yet.

2.5 Semi-Analytical Solutions Including Combined Excitation Mechanisms

The vibration of cylinders in a tube bank is different from a collection of vibrating cylinders in isolation. More complicated mathematical models to account for coupled vibration of cylinders in tube banks were proposed by Blevins [18], Chen [45], and Price and Paidoussis [46]. In all of these models, cylinders were represented by Euler Beams and the interaction between vibrating cylinders was included in the governing equations by specifying the forcing functions to linearly depend on the displacements and velocities of cylinders. It was also assumed in these models that the amplitude of vibration is small enough so that the flow field is not disturbed due to vibration of cylinders. These models successfully describe the coupled vibration mode between cylinders, but can not be used with confidence for problems with large amplitude vibrations which lead to mechanical wear, fretting, corrosion, and fatigue failure of tube banks.

Blevins [18] considered "whirling" of a row of cylinders subjected to flows with low reduced velocities so that whirling vibration of cylinders is mainly due to lift force (caused by the asymmetry of flow pattern due to displacement of cylinders) and drag force. Other vibration inducing mechanisms were excluded from his analysis. The flow velocity for the onset of whirling instability could be obtained from the analysis.

Chen [45] considered vibration of a row of cylinders subjected to a multiple number of excitation forces such as vortex shedding, fluidelastic coupling, drag and lift forces, and fluid inertia coupling. Apparently his model can be extended to vibration of tube banks with multiple rows once the fluid force coefficients for all the cylinders in the tube bank are provided by experiments or by other means, for example, computational fluid dynamics. The mathematical model due to Chen [45] is discussed below, for its generality and completeness.

HEAT EXCHANGER

OXIDIZER PREBURNER

MAIN INJECTOR

HOT GAS MANIFOLD ASSEMBLY

FUEL PREBURNER
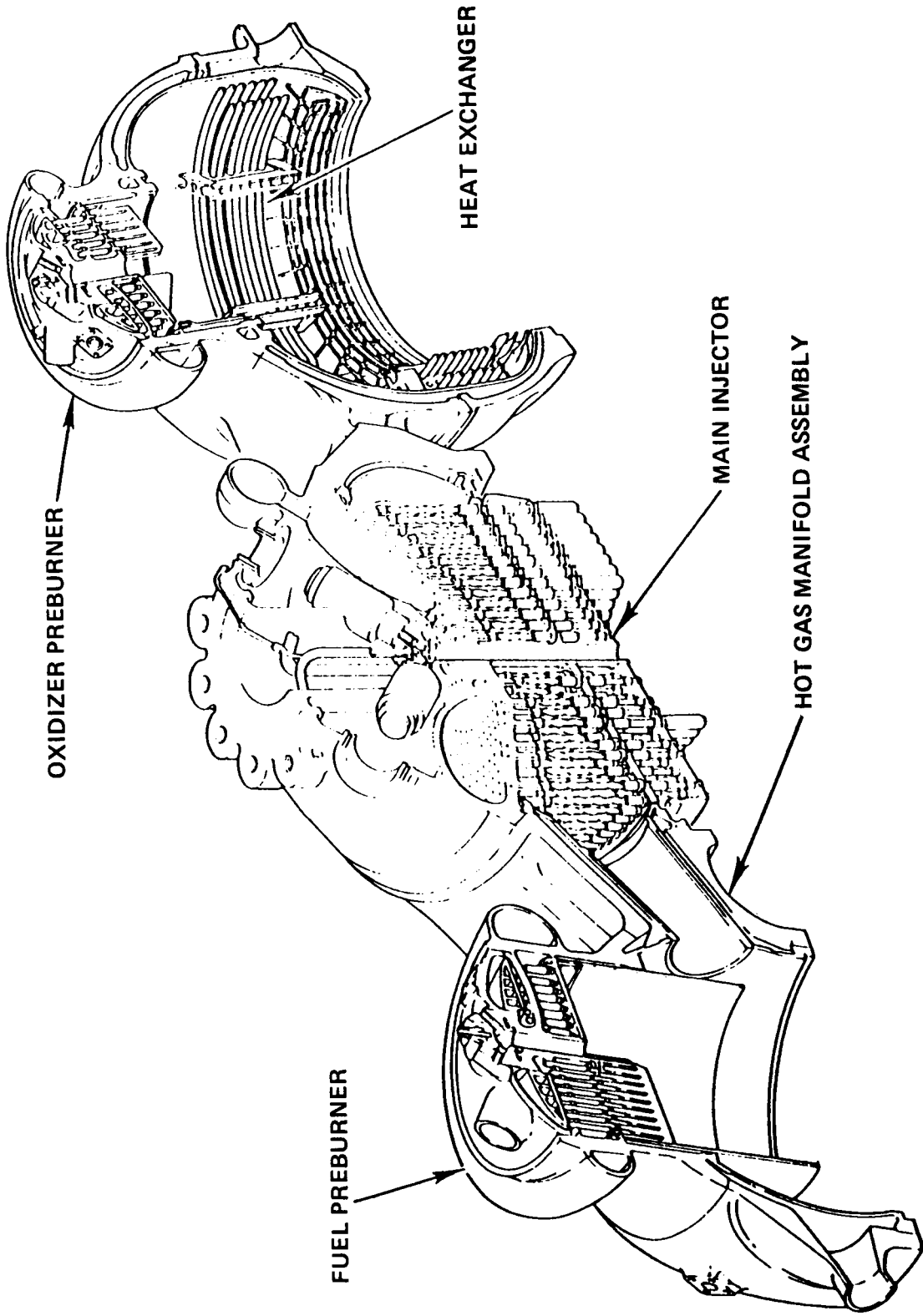
Figure 7. Space Shuttle Main Engine (SSME) power head assembly.

F: FUEL SIDE, OX: OXIDIZER SIDE
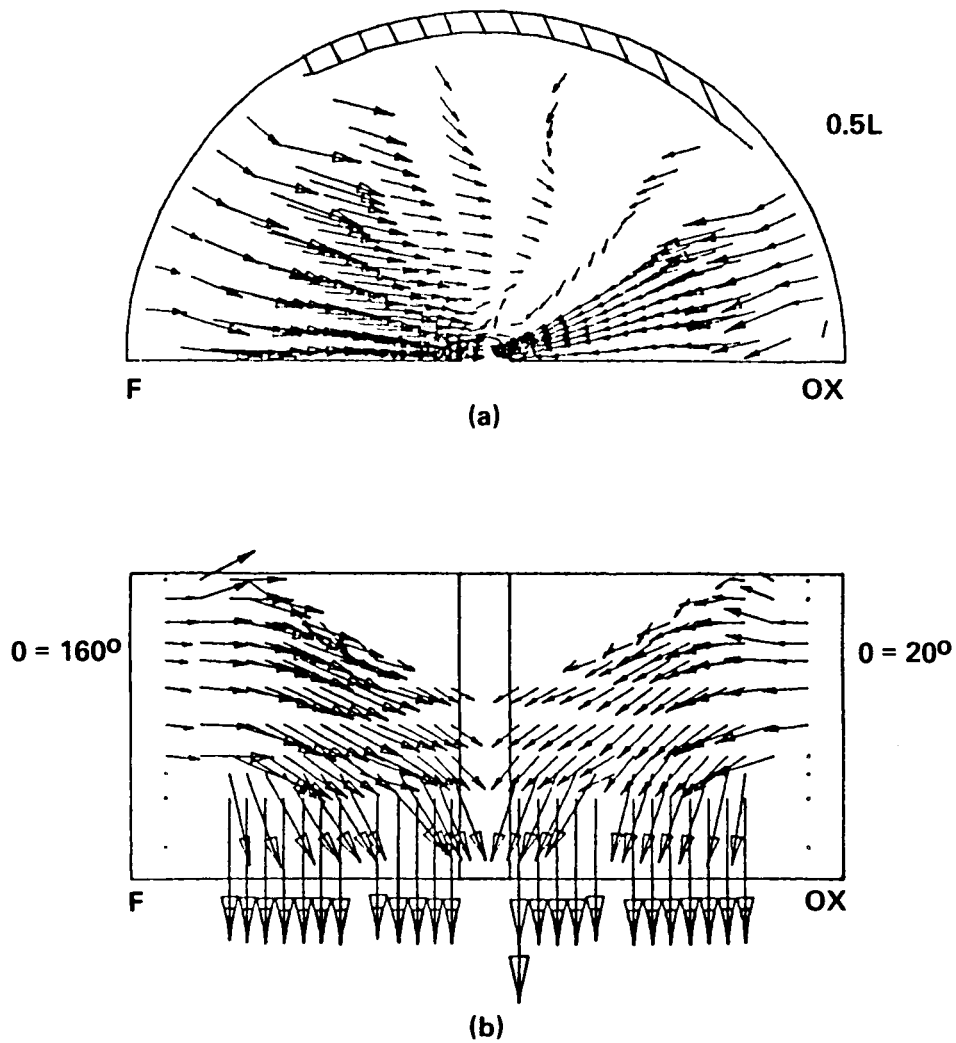
Figure 8. Flow field inside the SSME Main Injector Assembly [44].
(a) Horizontal velocity profile on the middle plane. (b) Vertical
velocity profile at 30 deg plane from center line.

The equation of motion for a single cylinder, which has the same flexural rigidities in both flow direction and transverse to the flow direction, can be written as [45]:

$$E_i \ I_i \ \frac{\partial^4 \underset{\sim}{u_i}}{\partial \ell^4} + c_i \ \frac{\partial \underset{\sim}{u_i}}{\partial t} + m_i \ \frac{\partial^2 \underset{\sim}{u_i}}{\partial t^2} = \underset{\sim}{f_i} \tag{2.9}$$

where the subscript i denotes the ith cylinder in the tube bank, ℓ is measured along the cylinder axis, E is the modulus of elasticity, I is the area moment of inertia, $\underset{\sim}{u}^T = (u_1, u_2)$, u_1 is the displacement in the flow direction (hereafter denoted as x-coordinate direction), u_2 is the displacement in the transverse direction (hereafter denoted as y-coordinate direction), $\underset{\sim}{f}^T = (f_x, f_y)$, f_x and f_y are forcing functions. The major difficulty in flow-solid interaction analysis lies in determining the forcing functions which depend on the displacement of cylinders. Chen [45] decomposed the forcing function as:

$$\underset{\sim}{f_i} = \underset{\sim}{f_i}{}^c + \underset{\sim}{f_i}{}^\ell + \underset{\sim}{f_i}{}^e + \underset{\sim}{f_i}{}^h + \underset{\sim}{f_i}{}^o \tag{2.10}$$

where

$$\underset{\sim}{f_i}{}^c = - M' \ \alpha_{ij} \ \frac{\partial^2 \underset{\sim}{u_j}}{\partial t^2} \tag{2.11}$$

$$\underset{\sim}{f_i}{}^\ell = \frac{1}{2} \rho \ V^2 \ d \ \left\{ \begin{array}{l} c_i{}^\ell \ \sin(\omega_s t + \psi_i{}^\ell) \\ c_i{}^d \ [1 + \varepsilon_i \ \sin(2 \ \omega_s t + \psi_i{}^d)] \end{array} \right\} \tag{2.12}$$

$$\underset{\sim}{f_i}{}^e = \frac{1}{2} \rho \ V^2 \ d \ (\mu_{ij} \ u_{ij} + \nu_{ij} \ u_{2j}) \tag{2.13}$$

$$\underset{\sim}{f_i}{}^h = -\rho \ V \ d \ (s_{ij} - \dot{u}_{ij} + t_{ij} \ \dot{u}_{2j}) \quad . \tag{2.14}$$

In equations (2.10) through (2.14), $\underset{\sim}{f_i}{}^c$ is the inertia force of fluid displaced by vibration of cylinders, M' is mass of displaced fluid, α_{ij} is added mass coefficients for ith cylinder due to displacement of jth cylinder; $\underset{\sim}{f_i}{}^\ell$ is the column vector of drag force in x-direction and lift force in y-direction, $c_i{}^\ell$ is the lift coefficient, $c_i{}^d$ is the drag coefficient, ε_i is a small number to be determined experimentally, ω_s, $\omega_s = 2\pi S/d$, is the vortex shedding frequency, $\psi_i{}^\ell$ and $\psi_i{}^d$ are phase delay angles for lift and drag

16

forces, respectively; $\underset{\sim i}{f}^e$ is a column vector of fluidelastic forces, μ_{ij} is the fluid-elastic force coefficients; $\underset{\sim i}{f}^h$ is the hydrodynamic damping forces, s_{ij} and t_{ij} are hydrodynamic damping coefficients; and $\underset{\sim i}{f}^o$ is a column vector of forcing functions due to the rest of vibration inducing mechanisms. Equations (2.9) and (2.10) are quite general so that response of cylinders due to a specific vibration mechanism or any set of combined mechanisms can be analyzed by simplifying the load term, equation (2.9). But the quality of analysis will depend on the physical coefficients used in equations (2.9) and (2.10). A set of analytical solutions, using the Eigen value analysis method, for natural frequencies and mode shapes of coupled vibrations, critical flow velocities for different excitation forces, and response to vortex shedding, lift, and drag forces for a row of cylinders have been presented in Reference 45.

Prices and Paidoussis [46] considered vibration of two rows of cylinders in cross flow. Fluid force ciefficients used in the analysis were obtained from wind tunnel tests [47,48]. The form of governing equation of motion used in their analysis is the same as that of Chen [45]. But they elaborated on modeling the effect of fluid retardness and time delay. The results showed that: analysis of a single flexible cylinder in a tube bank of rigid cylinders yielded reasonably good approximation of critical flow velocity for tube banks with all flexible cylinders for $m\delta/\rho d^2$ less than 300, but not for $m\delta/\rho d^2$ greater than 300. Also, based on their analytical analysis, they recommended to separate δ from $m/\rho d^2$ in the experimental correlation equations, as in equation (2.5).

III. NUMERICAL ANALYSIS METHODS FOR FLOW-SOLID INTERACTIONS

Geometrical and material nonlinearity inherent to flow-solid interaction phenomena precludes the possibility of obtaining closed form solutions to these problems except for simplified cases. It would be desirable to predict the flow-solid interactions numerically by solving unsteady turbulent flow equations, i.e., unsteady Navier-Stokes equations with appropriate turbulence models. By obtaining the pressure distribution and skin friction on the surface of the structure, one could then solve structural dynamics equations for vibration (and stability analysis) iteratively. The vibration inducing mechanisms such as vortex shedding, fluctuating turbulent wall pressure, and jet switching may be obtained as part of numerical solution.

Significant progress in numerical modeling of flow-solid interactions, turbulence models, and nonlinear structural analysis methods has been made recently. Existing literature covers: unsteady turbulent flows around rigid bodies and/or rigid containers; fully coupled laminar flow-solid interactions; and nonlinear stability, vibration, and elasto-viscoplastic analysis of structures subjected to known applied loads. For turbulent flow-solid interaction cases, the applied loads due to fluid flow have been obtained by solving the turbulent flow equations separately or by incorporating analytical or experimental correlation equations for fluctuating wall pressures induced by turbulence. Fully coupled numerical analysis of flow-solid interaction in cross flows, either laminar or turbulent, for a nest of cylinders has not been made yet.

Some of the numerical analysis methods for laminar flow-solid interactions, turbulent flow-solid interactions, mathematical models of turbulence, and structural

analysis methods which may be relevant to developing numerical methods for a class of flow-solid interaction of a nest of cylinders subjected to cross flows are discussed below.

3.1 Laminar Flow-Solid Interactions

Most of the recent investigations using numerical analysis for flow-solid interactions have been intended for safety analysis of nuclear reactors exposed to transient fluid loading. In these problems, displacements excursed by fluid particles and surrounding or submerged structures are of the same order of magnitude, and the time period of interest is very short (a few milliseconds for some cases). The effect of turbulent viscosity has not been included in these models. Researchers in this area developed a special mathematical model and numerical analysis methods which are suitable for this special class of flow-solid interaction problems. The governing equations are described in Lagrangian-Eulerian coordinate system which was originally proposed by Noh [49] and further developed by Hirt [50] to be used for all flow velocities. The advantages of the Lagrangian-Eulerian description are: excessive distortion of computational grids can be avoided; and grid points can be displaced independently of the fluid motion so that implementation of fluid-structure interface condition can be simplified.

Let $v_j (j=1,2,3)$ be the velocity vector of a fluid particle, v_j^G be the grid velocity vector, and v_j^D be the difference velocity vector defined as:

$$v_j^D = v_j - v_j^G \quad , \tag{3.1}$$

where j denotes the spatial coordinate directions. Then the governing equations for the fluid flow in the Lagrangian-Eulerian coordinate system are obtained to be:

$$\frac{\partial \rho}{\partial t} + v_j^D \frac{\partial \rho}{\partial x_j} + \rho \frac{\partial v_j}{\partial x_j} = 0 \tag{3.2}$$

$$\rho \left(\frac{\partial v_i}{\partial t} + v_j^D \frac{\partial v_i}{\partial x_j} \right) - \frac{\partial}{\partial x_j} \delta_{ij} - \rho b_i = 0 \tag{3.3}$$

$$\rho \left(\frac{\partial e}{\partial t} + v_j^D \frac{\partial e}{\partial x_j} \right) - \delta_{ij} \frac{\partial v_i}{\partial x_j} = 0 \tag{3.4}$$

$$\delta_{ij} = -p \, \delta_{ij} + \mu \left(\frac{\partial v_i}{\partial x_j} + \frac{\partial v_j}{\partial x_i} \right) \quad , \tag{3.5}$$

where equations (3.2) through (3.5) represent conservation of mass, linear momentum, energy, and constitutive equations respectively, ρ is the density, σ_{ij} is the fluid

18

stress tensor, b_i is the component of the body force along the ith coordinate direction, e is the internal energy, μ is the molecular viscosity, and p is the pressure.

Finite element representation of equations (3.2) through (3.5) are all based on the same method of weighted residuals, but detailed solution techniques used by different groups of workers, i.e., Donea et al. [51], Belytschko et al. [52,53], and Liu [54], are somewhat different.

In the finite element method, each variable is interpolated using shape functions and nodal values of these variables. These are:

$$v_i(\underset{\sim}{x},t) = v_{ik}(t)\ \phi_k(\underset{\sim}{x}) \quad , \qquad k = 1,\ N_k \qquad\qquad (3.6)$$

$$v_i^G(\underset{\sim}{x},t) = v_{ik}^G(t)\ \phi_k(\underset{\sim}{x}) \quad , \qquad k = 1,\ N_k \qquad\qquad (3.7)$$

$$\rho(\underset{\sim}{x},t) = \rho_m(t)\ \Phi_m(\underset{\sim}{x}) \quad , \qquad m = 1,\ N_m \qquad\qquad (3.8)$$

$$\rho e(\underset{\sim}{x},t) = (\rho e)_m\ \Phi_m(\underset{\sim}{x}) \quad , \qquad m = 1,\ N_m \qquad\qquad (3.9)$$

$$P(\underset{\sim}{x},t) = P_s(t)\ \chi_s(\underset{\sim}{x}) \quad , \qquad s = 1,\ N_s \qquad\qquad (3.10)$$

where the shape functions $\phi_k(x)$, $\Phi_m(x)$, and $\chi_s(x)$ are functions of spatial coordinates; nodal values of these variables are functions of time; and N_k, N_m, and N_s denotes number of these variables for each element. In general, the order of interpolating polynomials and inter-element continuity requirements are different depending on the differential equations to be solved and the numerical method employed. The finite element system of equations are obtained by multiplying the differential equations with appropriate test functions, substituting the continuous variables with interpolated expressions, integrating over an element, and assembling the resulting element system of equations into a global system of equations.

Donea et al. [51] used linear shape functions for the velocities, and constant elements for density and internal energy. In this method, the pressure, p, was determined using an explicit relationship of the form $p = p(\rho,e)$. Consequently, p is constant in each element and the shape function χ was not used in his case. Also a special form of interpolation as given in equation (3.9) was used for internal energy in [51]. The finite element system of equations due to Donea et al. [51] is as follows:

$$\underset{\sim}{D}\rho = \underset{\sim}{f}^\rho \qquad\qquad (3.11)$$

$$\underset{\sim}{M}v_i = \underset{\sim}{f}_i^V \qquad\qquad (3.12)$$

$$\underset{\approx}{E}(\rho e) = \underset{\sim}{f}^{e} \tag{3.13}$$

in which each of the entries in the above matrices are given by:

$$D_{mn} = \int_{\Omega_e} \Phi_m \, \Phi_n \, d\underset{\sim}{x} \tag{3.14}$$

$$M_{k\ell} = \int_{\Omega_e} \rho \, \phi_k \, \phi_\ell \, d\underset{\sim}{x} \tag{3.15}$$

$$E_{mn} = \int_{\Omega_e} \Phi_m \, \Phi_n \, d\underset{\sim}{x} \tag{3.16}$$

$$f_m^{\rho} = \int_{\Omega_e} \Phi_m \left(- v_j^D \frac{\partial \rho}{\partial x_j} - \rho \frac{\partial v_j}{\partial x_j} \right) d\underset{\sim}{x} \tag{3.17}$$

$$f_{ik}^{v} = \int_{\Omega_e} \phi_k \left(- \rho \, v_j^D \frac{\partial v_i}{\partial x_j} + \rho \, b_i \right) d\underset{\sim}{x} + \int_{\Omega_e} p \, \frac{\partial \phi_k}{\partial x_i} \, dx + \int_{\Omega_e} \phi_k \, T_i \, ds \tag{3.18}$$

$$f_m^{e} = \int_{\Omega_e} \Phi_m \left\{ - v_j^D \frac{\partial (\rho e)}{\partial x_j} - (\rho e + p) \frac{\partial v_j}{\partial x_j} \right\} d\underset{\sim}{x} \quad . \tag{3.19}$$

In equations (3.10) through (3.13), D and E are diagonal matrices due to the shape functions used and the mass matrix M was made to be a diagonal matrix using a lumping method [55]. In equations (3.14) through (3.19), Ω_e denotes an element, $\partial \Omega_e$ denotes the boundary of the same element, T_i denotes the applied surface traction, and the rest of the notations are the same as before. The dissipation term due to molecular viscosity, $\mu(\partial v_i / \partial x_j + \partial v_j / \partial x_i)$, was neglected from the conservation of linear momentum equation, equation (3.3). The resulting discrete system of equations for this inviscid flow field was integrated in time direction using a predictor-corrector method.

The structural domain was discretized into a number of conical shell elements [57] and a time dependent elasto-plasticity finite element method developed by Belytschko and Hsieh [57] was used for structural analysis in Donea et al. [51]. The structural analysis part will be discussed separately in Section 3.4.

One of the example problems considered in Reference 51 was a thin cylinder vessel, with hemispherical bottom almost completely filled with water, subjected to blast loading from inside. The system of equations were integrated in time up to a few milliseconds. The physical problem and the computational results are shown in Figure 9 together with moving finite element meshes. Since no viscosity was included in Reference 51, a slipping flow boundary condition was used for tangential velocity; and the normal velocity was prescribed to be the same as the normal component of the moving boundary. This again is obtained as a part of numerical solution at each time-level.

The finite element method for flow analysis used by Belytschko et al. [51,53] is basically the same as the one used in Reference 51, but he used an averaging method for each of the variables in an element so that the element mass matrix would be a diagonal matrix. He also used an hourglass control algorithm to avoid zero-energy mode resulting from the averaging method. In this case, the load vector f^V contains an extra term contributed by the hourglass control algorithm in addition to the usual load vectors due to convection, molecular diffusion, surface tensions, and body forces. The system of equations was integrated in time-direction, using an explicit time integration method, up to a few milliseconds in a finite element modeling of hypothetical nuclear reactor core disruptive accident. Their computational results compared favorably with the experimental displacement data. In the experiment, permanent plastic deformation and severe buckling of steel columns were reported. In order to model the buckling of steel columns in the numerical analysis, a slight imperfection had been included in the geometry data of the steel column. The structural analysis method used can be found in Reference 57.

Liu solved the same set of flow equations using the penalty method to exclude the conservation of mass equation and pressure variable from the system of equations. The penalty method has been used very frequently for incompressible laminar flow problems [58] and the Stoke's problem [59]. In his method, the stress term, equation (3.5), was considered as an extra variable and was interpolated separately, which is called the mixed finite element method. He included an elasto-viscoplasticity model in the structural analysis part to cover strain rate sensitive solid materials. The elasto-viscoplasticity model is covered separately in Section 3.4.

As can be noticed, there exists significant difference between the nuclear reactor safety analysis problems and the flow-solid interaction of a nest of cylinders in cross flows. In the latter problem, it is very important to include the turbulent viscosity into the flow equations. Any cylinder of a tube bank subjected to cross flows will vibrate with respect to its equilibrium position. Even at the onset of failure due to large deformation, the distance excursed by any cylinder is small compared to the distance traveled by a fluid particle. For these reasons, direct use of the Langrangian-Eulerian description may not be necessary for flow-solid interaction analysis of a nest of cylinders in cross flows. But the concept of Lagrangian-Eulerian description can be used advantageously to obtain convergent solutions for convection dominated flows as has been pointed out by Zienkiewicz [58].

3.2 Turbulent Flow-Solid Interactions

Coupled and uncoupled turbulent flow-compliant material interactions were studied numerically by Buckingham et al. [16,17] in an effort to reduce drag and aeroacoustic noise of submersible hulls. Uncoupled analysis was used to eliminate a number of
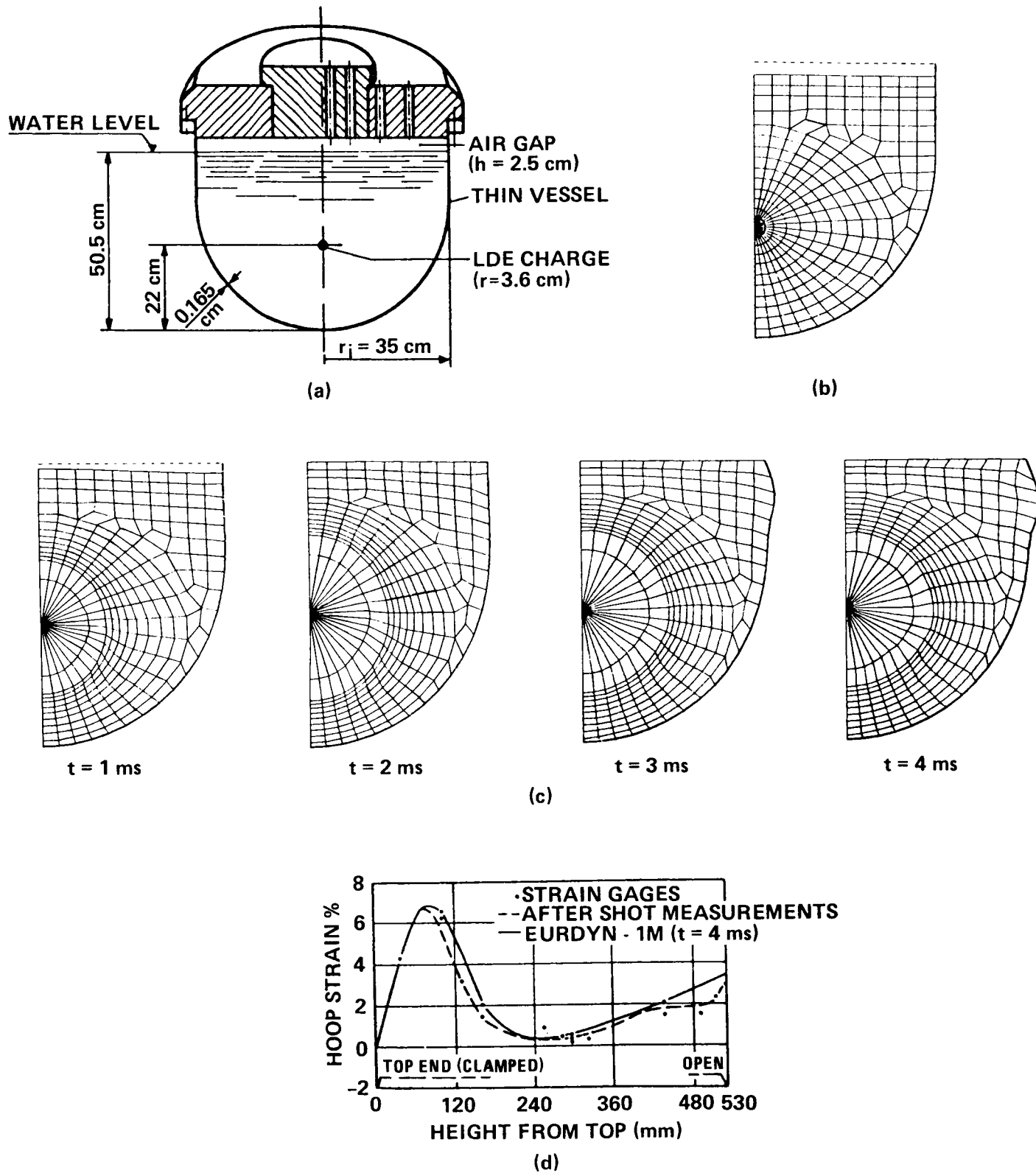
Figure 9. Finite element analysis of a nuclear reactor safety problem [51].
(a) Description of the physical problem. (b) Discretized computational
domain. (c) Deformed configurations at t = 1, 2, 3,
and 4 ms. (d) Computational result.

candidate compliant materials and internal structures (Fig. 10) which do not exhibit the desired vibration response from the more elaborate and time consuming fully coupled flow-solid interaction analysis. Different materials considered include polyvinylchloride, rubbers, and many others. For all the cases of coupled and uncoupled turbulent flow-compliant material interactions considered in References 16 and 17, the structural dynamics equation was solved by the finite element codes due to Hallquist [60,61]. An elastic or a linear viscoelastic constitutive equation [62] were used to model the compliant materials. These constitutive equations and the finite element method for structural dynamics are discussed in Section 3.4.
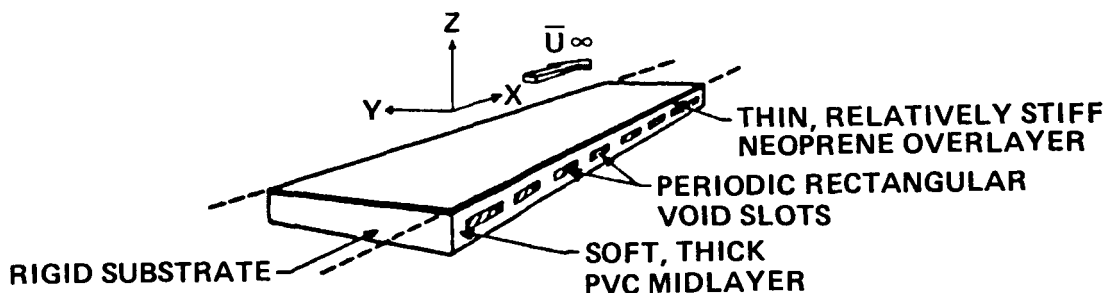
Figure 10. Geometry of compliant surfaces, flow and coordinate system for finite element transient response simulation [16,17].

In the uncoupled analysis, the fluctuating turbulent wall pressure was generated using the Ash code [13,14]. Ash code can generate fluctuating turbulent wall pressure beneath fully turbulent boundary layer flows. In the method, the instantaneous pressure at a spatial and temporal location is obtained by summing up all the pressure events affecting the location. Information required to generate each of the pressure events include: root mean square value of fluctuating turbulent wall pressure, p_{rms} (or turbulent wall shear stress and its relationship to p_{rms}); probability distribution of time between pressure events; probability distribution of frequencies for the pressure events; convection speed of the pressure events; decay ratio of amplitude of pressure events; wave form of pressure carriers; and etc. In the work of Ash [13,14], all this information was obtained from several different sets of experimental data for turbulent boundary layer flows; and the statistical results of the generated fluctuating turbulent wall pressure compared favorably with experimental data. Universality of these experimental correlation equations for different flow situations need to be examined further. In order to simulate the fluctuating turbulent wall pressure, much statistical information must be known priori for the flow field, therefore his method is of limited use for general flow situations [13].

In the fully coupled case [16,17], both the two- and three-dimensional Navier-Stokes equations were solved by a pseudo-spectral method [63,64] developed by Orszag and Kells [63,64]. The pseudo-spectral method [63,64] was originally developed to solve the Navier-Stokes equations for finite amplitude disturbances in order to predict transition criterion from laminar to turbulent flow of plane Poiseuille and plane Couette flows. The flow field, considered in References 16 and 17, is governed by the incompressible Navier-Stokes equations:

$$\underset{\sim}{\nabla} \cdot \underset{\sim}{v} = 0 \qquad\qquad\qquad (3.20)$$

$$\frac{\partial \underset{\sim}{v}}{\partial t} + (\underset{\sim}{v} \cdot \underset{\sim}{\nabla}) \underset{\sim}{v} = -\underset{\sim}{\nabla}P + \nu\nabla^2 \underset{\sim}{v} \tag{3.21}$$

$$0 \leq x \leq X \quad , \quad 0 \leq y \leq Y \quad , \quad \text{and} \quad 0 \leq z \leq Z \tag{3.22}$$

where equation (3.20) is the conservation of mass equation; equation (3.21) is the conservation of linear momentum equation; equation (3.22) is the domain of the problem; $\underset{\sim}{v}^T = (v_1, v_2, v_3)$ is a column vector of velocities in the three spatial coordinate directions; $\underset{\sim}{\nabla}$ is the gradient operator; and X, Y, and Z denote extension of the domain. The domain in the z-direction was set at a distance of several boundary layer thicknesses away from the wall so that the free stream boundary condition can be used at the outer edge of the domain. The fluid particles at the flow-compliant material interface were set to move together in the normal direction, i.e., the flow velocity in the normal to the surface of compliant material direction is dictated by the normal velocity of the compliant material which is obtained from the structural dynamics solution but the flow velocities in both of the tangential to the surface directions were set equal to zero. In the free stream flow direction, a cyclic boundary condition such that $v(0,y,z) = v(X,y,z)$ was used. In Orszag et al. [63,64], the Navier-Stokes equation was first rewritten in a rotational form given as:

$$\frac{\partial \underset{\sim}{v}}{\partial t} = \underset{\sim}{v} \times \underset{\sim}{\omega} - \underset{\sim}{\nabla} \left(P + \frac{1}{2}\left|\underset{\sim}{v}\right|^2\right) + \nu\nabla^2\underset{\sim}{v} \quad , \tag{3.23}$$

where $\underset{\sim}{\omega}(\underset{\sim}{x},t)$, $\underset{\sim}{\omega}(\underset{\sim}{x},t) = \underset{\sim}{\nabla}\times\underset{\sim}{v}(\underset{\sim}{x},t)$, is the curl of the velocity vector, and the rest of the notations are the same as before. Equation (3.23) was solved by a pseudo-spectral method. The pseudo-spectral method has also been used quite frequently in the large eddy simulation method which will be discussed in the next section. Therefore, a brief explanation and a discussion on the advantages and disadvantages of the method is given below.

The pseudo-spectra method they used belongs to the classical collocation method. In the collocation method, solution to the governing differential equations are interpolated using basis polynomials and constant coefficients assigned to each of the polynomials. In their case, the velocity field was represented by:

$$\underset{\sim}{v} = \sum_{|m|<M} \sum_{|n|<N} \sum_{p=0}^{P} a(m,n,p,t) \, T_p(z) \, e^{[2\pi_i(mx/X + ny/Y)]} \quad , \tag{3.24}$$

where m, n, and p are integers so that a set of (m,n,p) designate each collocation point; (2M), (2N), and (P+1) are the number of collocation points in each of the spatial coordinate directions respectively; $a(m,n,p,t)$ is function of time only, and $T_p(z)$, $T_p(z) = \cos(p\cos^{-1}z)$, is the Chebyshev polynomial of degree p. Substituting equation (3.24) into equation (3.2.4) and collocating at each of the collocation points

24

yields a system of nonlinear ordinary differential equations, which can be solved by any nonlinear ordinary differential equation solution method. But a straight forward computation of the collocation method requires enormous computational time as the number of collocation points is increased. The special features of the pseudo-spectral method due to Orszag et al [63,64] are: orthogonality of the basis polynomials is best utilized by performing most of the computations in the Fourier transformed space and then mapped back onto the physical space using the fast Fourier Transformation method [65] so that the required number of computations are reduced by orders of magnitude; and the Adams-Bashforth-Crank-Nicholson time itnegration method devised to be used in the pseudo-spectral method is one of the best time integrators for ordinary differential equations with regard to truncation errors and numerical stability requirement. Detailed explanation on the computational procedure of the pseudo-spectral method can be found in a number of literatures [66,67,68]; therefore, it is not discussed herein.

In order to use the pseudo-spectral method to solve any ordinary or partial differential equations, basis polynomials which span entire domain and satisfy the prescribed boundary conditions must be available a priori. Due to this difficulty, the pseudo-spectral method has been used mainly for channel flows or axisymmetric annular flows where cyclic boundary conditions can be specified for the upstream and the downstream locations. The validity of cyclic boundary conditions has been questioned in References 67, 68, and 80. The boundary conditions are believed to be approximately applicable for fully developed channel or pipe flows [63,64,92]. Accordingly, the method may be suitable for problems with extremely limiting cases of boundary conditions defined on simple regular domains. Application of the method to flow-solid interaction analysis of a nest of cylinders subjected to cross flows would be extremely difficult, if not impossible, due to the complicated domains and boundary conditions.

3.3   Turbulence Models

In numerical analysis of a nest of cylinders subjected to cross flows, pressure straining and redistribution of Reynolds stresses near the wall region may become important due to a number of cylinders in the cross flow. Also in flow-solid interactions, fluid force is transmitted to the structure through wall pressure and skin friction; therefore, evaluation of fluctuating turbulent wall pressure is very important. Since successful numerical analysis of flow-solid interaction of tube banks would require an appropriate unsteady turbulence model to be incorporated into the flow analysis, a few turbulence models are discussed below.

Significant progress has been made in modeling steady turbulent flows. But due to pressure straining, redistribution of Reynolds stresses, and the complicated geometry of tube banks, some of the steady state turbulence models with proven performance may not even be applicable for steady turbulent flows through a nest of rigid cylinders. For example, low Reynolds number turbulence models which include the distance from the walls explicitly in the turbulence equations may hardly be applicable for flows through tube banks, since there exist so many cylinder walls in any tube bank, e.g., there are 600 tubes in the SSME Main Injector Assembly. On the other hand, numerical modeling of unsteady turbulent flows has shorter history than the steady case; consequently, there exist only a limited number of publications in this area and physical understanding of unsteady turbulent flows is not complete at the present time. Therefore, this discussion is limited to the most successful turbulence models which may be further extended to unsteady turbulent flows and which can be

used for turbulent flow-solid interaction of tube banks. These are a few low Reynolds number k-ε turbulence models, a few different versions of the algebraic Reynolds stress models, and the large eddy simulation method (LES). The LES method cannot be used for turbulent flows through tube banks at its present state of development as can be seen in the following discussions, but the method has been originally developed for and primarily used for unsteady turbulent flows. Comprehensive reviews of various turbulence models can be found in Nallasamy [69], Martin [70], Lakshminarayana [71], and the references appearing in these literatures.

3.3.1. Extended k-ε Turbulence Models and Algebraic Reynolds Stress Models

For a class of complex flow problems, anisotropy of Reynolds stresses induce significant differences in the predicted flow field, e.g., the existence of secondary flow in curved square ducts [72]. For these flows, the conventional (or standard) k-ε turbulence model yields unsatisfactory computational results. The Reynolds stress model [73] can describe the convection, diffusion, and anisotropy of each component of the Reynolds stresses. But use of the Reynolds stress model is prohibited in many cases of practical importance due to the number of variables which result from six differential equations for Reynolds stresses and one equation for turbulence dissipation function for three-dimensional flows.

In order to account for the anisotrophy of Reynolds stresses, the algebraic stress model, which retains most of the basic features of the original Reynolds stress model, was developed [74]. The algebraic relationship between the six Reynolds stress components are obtained from the Reynolds stress equation by neglecting the convection and diffusion terms [76] or by assuming the convective transport of Reynolds stresses to be proportional to the transport rate of turbulent kinetic energy [74]. Hence in algebraic Reynolds stress models, the k-ε turbulence models are enhanced with this algebraic relationship instead of using the classical Boussinesq eddy viscosity assumption [76].

In the numberical analysis of turbulent flows, the wall boundary conditions are usually applied in two different ways. In the first approach, the computational boundary of flow domain near the wall is slightly separated from the wall and the wall functions are applied at the first grid point. Strictly speaking, these wall functions are not applicable near the separation points on the walls; nevertheless, they have been used successfully in many cases. In the second approach, the first grid point is located on the wall, no slip boundary condition is applied at the grid point, and the necessary modifications are included in the turbulence models in order to account for the low Reynolds number effect near the wall.

In flow-solid interaction of a nest of cylinders subjected to cross flows, the vibration of cylinders is a three-dimensional motion. The capability of wall function methods for the analysis of flows with moving boundaries has not been established as yet, and need to be established so that the method can be used for the analysis of flow-solid interactions. Alternatively, the low Reynolds number turbulence model may be used so that the no-slip flow boundary conditions can be specified at the flow-solid interfaces.

For unsteady turbulent flows, the mean and fluctuating quantities are defined differently than those for steady turbulent flows. Therefore, it would be appropriate to include this topic. The most familiar averaging technique for unsteady turbulent flows would be the ensemble averaging method in the sense that it yields exactly the

26

same flow equations as the time averaging method for steady turbulent flows. Ensemble average of any fluctuating quantity, $\Psi(x,t)$, is defined as:

$$\overline{\Psi}(\underset{\sim}{x},t) = \lim_{N \to \infty} \sum_{n=0}^{N} \Psi(\underset{\sim}{x} + n\tau) \tag{3.25}$$

where τ is the period of fluctuation, n is an integer, and $\overline{\Psi}$ denotes ensemble average of Ψ. On the other hand, the time average for steady turbulent flows is defined as

$$\widehat{\Psi}(\underset{\sim}{x},t) = \lim_{T \to \infty} \frac{1}{T} \int_{t}^{t+T} \Psi(\underset{\sim}{x},t) \, dt \tag{3.26}$$

where $\widehat{\Psi}$ denotes the averaged quantity. For both of the averaging techniques, the velocity component is decomposed as

$$\underset{\sim}{v} = \overline{\underset{\sim}{v}} + \underset{\sim}{v}' \tag{3.27}$$

where $\underset{\sim}{v}^T = (v_1, v_2, v_3)$ is a column vector of the three velocity components in the three spatial coordinate directions, and $\underset{\sim}{v}'$ is the corresponding column vector of the fluctuating velocities. The time dependent turbulent flow equations for incompressible flows are given as:

$$\frac{\partial \overline{v}_j}{\partial x_j} = 0 \tag{3.28}$$

$$\rho \left(\frac{\partial \overline{v}_i}{\partial t} + v_j \frac{\partial \overline{v}_i}{\partial x_j} \right) = - \frac{\partial \overline{P}}{\partial x_i} + \frac{\partial}{\partial x_j} \left(\mu \frac{\partial \overline{v}_i}{\partial x_j} \right) - \frac{\partial (\overline{\rho v_i' v_j'})}{\partial x_j} \quad . \tag{3.29}$$

The Reynolds stress, $\overline{v_i' v_j'}$, in equation (3.29) is modeled using the Boussinesq viscosity assumption given as:

$$-\overline{v_i' v_j'} = \nu_t \left(\frac{\partial \overline{v}_i}{\partial x_j} + \frac{\partial \overline{v}_j}{\partial x_i} \right) - \frac{2}{3} \delta_{ij} k \quad , \tag{3.30}$$

where ν_t is the turbulent viscosity; δ_{ij} is the Kronecker delta such that $\delta_{ij} = 1$ for $i = j$, and $\delta_{ij} = 0$ for $i \neq j$; and k is the turbulent kinetic energy, $k = 1/2 \, \overline{v_i' v_i'}$.

27

The standard two equation (k-ε) turbulence model due to Launder and Spalding [78] is given as:

$$\frac{\partial k}{\partial t} + \overline{v}_j \frac{\partial k}{\partial x_j} = \frac{\partial}{\partial x_j} \left(\frac{\nu_t}{\sigma_K} \frac{\partial k}{\partial x_j} \right) + P - \varepsilon \qquad (3.31)$$

$$\frac{\partial \varepsilon}{\partial t} + \overline{v}_j \frac{\partial \varepsilon}{\partial x_j} = \frac{\partial}{\partial x_j} \left(\frac{\nu_t}{\sigma_\varepsilon} \frac{\partial \varepsilon}{\partial x_j} \right) + c_{\varepsilon 1} \frac{\varepsilon}{k} P - c_{\varepsilon 2} \frac{\varepsilon^2}{k} \quad , \qquad (3.32)$$

where ε is the dissipation rate of the turbulent kinetic energy,

$$\varepsilon = \nu \, \overline{\frac{\partial v_i'}{\partial x_j} \frac{\partial v_i'}{\partial x_j}} \quad ;$$

P is the production rate of the turbulent kinetic energy,

$$P = \nu_t \left(\frac{\partial \overline{v}_i}{\partial x_j} + \frac{\partial \overline{v}_j}{\partial x_i} \right) \frac{\partial \overline{v}_i}{\partial x_j} \quad ;$$

ν_t, $\nu_t = c_\mu k^2 / \varepsilon$, is the same turbulent viscosity as used in equation (3.20); and $c_\mu = 0.09$, $c_{\varepsilon 1} = 1.44$, $c_{\varepsilon 2} = 1.92$, $\sigma_k = 1.0$, and $\sigma_\varepsilon = 1.3$ have been used in Reference 78. Since equations (3.31) and (3.32) are not valid in the viscous sub-layer region near the wall, where the molecular viscosity is dominant over the eddy viscosity, the wall function methods are used to supply wall boundary conditions for the differential equations [78]. There exist a few modified k-ε turbulence models to include low Reynolds number effects. The extended k-ε turbulence model due to Hassid and Poreh [79] is given as

$$\frac{\partial k}{\partial t} + \overline{v}_j \frac{\partial k}{\partial x_j} = \frac{\partial}{\partial x_j} \left\{ \nu + \frac{\nu_t}{\sigma_k} \left(\frac{\partial k}{\partial x_j} \right) \right\} + P - \varepsilon - 2\nu \frac{k}{y^2} \qquad (3.33)$$

$$\frac{\partial \varepsilon}{\partial t} + \overline{v}_j \frac{\partial \varepsilon}{\partial x_j} = \frac{\partial}{\partial x_j} \left\{ \nu + \frac{\nu_t}{\sigma_\varepsilon} \left(\frac{\partial \varepsilon}{\partial x_j} \right) \right\} + c_{\varepsilon 1} \frac{\varepsilon}{k} P$$

$$- [1 - 0.3 \exp(-R_t^2)] \frac{\varepsilon^2}{k} - 2\nu \left(\frac{\partial \sqrt{\varepsilon}}{\partial x_j} \right)^2 \qquad (3.34)$$

where $\nu_t = c_\mu k^2/\varepsilon$, $c_\mu = c_{\mu\infty} f_\mu$, $f_\mu = 1 - \exp(-0.0015 R_t)$, $R_t = k^2/(\nu\varepsilon)$ is the turbulent Reynolds number, and $c_{\mu\infty} = 0.09$. The model by Jones and Launder [80] is given as

$$\frac{\partial k}{\partial t} + \overline{v}_j \frac{\partial k}{\partial x_j} = \frac{\partial}{\partial x_j}\left\{\left(\nu + \frac{\nu_t}{\sigma_K}\right)\left(\frac{\partial k}{\partial x_j}\right)\right\} + P - \varepsilon - 2\nu\left(\frac{\partial k^{\frac{1}{2}}}{\partial x_j}\right)^2 \qquad (3.35)$$

$$\frac{\partial \varepsilon}{\partial t} + \overline{v}_j \frac{\partial \varepsilon}{\partial x_j} = \frac{\partial}{\partial x_j}\left\{\left(\nu + \frac{\nu_t}{\sigma_\varepsilon}\right)\left(\frac{\partial \varepsilon}{\partial x_j}\right)\right\} + c_{\varepsilon 1}\frac{\varepsilon}{k}P - 2\nu\nu_t\left(\frac{\partial^2 \overline{v}_i}{\partial x_j \partial x_k}\right)^2 - c_{\varepsilon 2}\frac{\varepsilon^2}{k}$$

$$(3.36)$$

where $c_\mu = c_{\mu\infty}\exp[-2.5/(1 + R_t/50)]$, $c_{\varepsilon 2} = c_{\varepsilon\infty}[1 - 0.3\exp(-R_t^2)]$, $c_{\mu\infty} = 0.09$, $c_{\varepsilon 1} = 1.45$, and $c_{\varepsilon\infty} = 2.0$, and rest of the notations are the same as in equations (3.33) and (3.34). The wall boundary conditions for the low Reynolds number turbulence equations are given as:

$$\left.\begin{array}{l} k = 0 \\ \\ \varepsilon = 0 \end{array}\right\} \qquad . \qquad (3.37)$$

Various algebraic relationships between Reynolds stresses can be obtained by introducing simplifying assumptions into the Reynolds stress equation [73,77]. These simplifying assumptions are: production and dissipation of turbulent kinetic energy are in equilibrium, transport of Reynolds stresses are proportional to the transport of turbulent kinetic energy, transport and diffusion of Reynolds stress are negligible, and any appropriate combination of these assumptions. The Reynolds stress equation [73,77] and the algebraic Reynolds stress model due to Rodi [74] are given below. The Reynolds stress equation [73,77] is given as:

$$\underset{(I)}{\underbrace{\frac{\partial \overline{v_i' v_j'}}{\partial t}}} + \underset{(II)}{\underbrace{v_\ell \frac{\partial \overline{v_i' v_j'}}{\partial x_\ell}}} = -\underset{(III)}{\underbrace{\left\{\overline{v_j' v_k'}\frac{\partial \overline{v}_i}{\partial x_k} + \overline{v_i' v_k'}\frac{\partial \overline{v}_j}{\partial x_k}\right\}}} + \underset{(IV)}{\underbrace{\frac{P}{\rho}\left(\overline{\frac{\partial v_i'}{\partial x_j}} + \overline{\frac{\partial v_j'}{\partial x_i}}\right)}}$$

$$+ \underset{(V)}{\underbrace{\frac{\partial}{\partial x_k}\left\{\nu\frac{\partial \overline{v_i' v_j'}}{\partial x_k} - \overline{v_i' v_j' v_k'} - \frac{P}{\rho}(\delta_{jk}v_i' + \delta_{ik}v_j')\right\}}} - \underset{(VI)}{\underbrace{2\nu\overline{\frac{\partial v_i'}{\partial x_k}\frac{\partial v_j'}{\partial x_k}}}} \quad , \qquad (3.38)$$

where (I) is the time rate of change, (II) is the convective transport, (III) is the stress production, (IV) is the pressure straining term, (V) is the diffusive transport, and (VI) is the dissipation of the Reynolds stresses. The closure model for higher

order terms for low Reynolds number flows proposed by Hanjalic and Launder [77] are given as

$$\overline{\frac{P}{\rho} \left(\frac{\partial v_j'}{\partial x_i} + \frac{\partial v_i'}{\partial x_j} \right)} = - c_1 \frac{\varepsilon}{k} (\overline{v_i' v_j'} - \frac{2}{3} \delta_{ij} k) - \frac{c_2 + 8}{11} (P_{ij} - \frac{2}{3} \delta_{ij} k)$$

$$- \frac{(30 c_2 - 2)}{55} k \left(\frac{\partial \overline{v}_i}{\partial x_j} + \frac{\partial \overline{v}_j}{\partial x_i} \right) - \frac{8 c_2 - 2}{11} (D_{ij} - \frac{2}{3} P \delta_{ij}) + \phi_{ij, \omega}$$

(3.39)

$$\phi_{ij, \omega} = \left\{ 0.125 \frac{\varepsilon}{k} (\overline{v_i' v_j'} - \frac{2}{3} k \delta_{ij}) + 0.015 (P_{ij} - D_{ij}) \right\} \frac{k^{3/2}}{\varepsilon x_2}$$

(3.40)

$$P_{ij} = - \left\{ \overline{v_i' v_j'} \frac{\partial \overline{v}_j}{\partial x_k} + \overline{v_j' v_j'} \frac{\partial \overline{v}_i}{\partial x_k} \right\}$$

(3.41)

$$D_{ij} = - \left\{ \overline{v_i' v_k'} \frac{\partial \overline{v}_k}{\partial x_j} + \overline{v_j' v_k'} \frac{\partial \overline{v}_k}{\partial x_i} \right\}$$

(3.42)

$$\overline{-v_i' v_j' v_k'} = c_s \frac{k}{\varepsilon} \left\{ \overline{v_k' v_\ell'} \frac{\partial \overline{v_i' v_j'}}{\partial x_\ell} + \overline{v_j' v_\ell'} \frac{\partial \overline{v_k' v_i'}}{\partial x_\ell} + \overline{v_i' v_\ell'} \frac{\partial \overline{v_j' v_k'}}{\partial x_\ell} \right\}$$

(3.43)

$$- \overline{\frac{P}{\rho} (\delta_{jk} v_i' + \delta_{ik} v_j')} = 0$$

(3.44)

$$\nu \overline{\frac{\partial v_i'}{\partial x_k} \frac{\partial v_j'}{\partial x_k}} = \frac{2}{3} \left\{ (1 - f_s) \delta_{ij} + \frac{\overline{v_i' v_j'}}{(2k/3)} f_s \right\}$$

(3.45)

$$\frac{\partial \varepsilon}{\partial t} + \overline{v}_\ell \frac{\partial \varepsilon}{\partial x_\ell} = c_\varepsilon \frac{\partial}{\partial x_k} \left(\frac{k}{\varepsilon} \overline{v_k' v_\ell'} \frac{\partial \varepsilon}{\partial x_\ell} \right) - c_{\varepsilon 1} \frac{\varepsilon}{k} \overline{v_i' v_k'} \frac{\partial \overline{v}_i}{\partial x_k} - c_{\varepsilon 2} \frac{\varepsilon^2}{k}$$

(3.46

where $P = \overline{-v_\ell' v_k'} (\partial \overline{v}_\ell / \partial x_k)$ is the rate of generation of turbulence energy by the mean strains; $f_s = (1 + R_t / 10)^{-1}$; $R_t = k^2 / (\nu \varepsilon)$ is the turbulent Reynolds number; and $c_1 = 1.5$, $c_2 = 0.4$, and $c_s = 0.11$ have been used in Reference 77. The turbulence dissipation function, ε, in equations (3.39) through (3.45) is determined by equation

(3.46) which is the convection-diffusion equation of the turbulence dissipation function. The pressure straining due to wall proximity, equation (3.40), was proposed in Reference 73 but was disregarded in Reference 77. The form of wall proximity equation, equation (3.40), is not appropriate for numerical analysis of turbulent flows through the tube banks due to the explicit appearance of the distance from the wall.

The algebraic Reynolds stress model derived by Rodi [74] is given below, where the convective transport term of the Reynolds stresses is assumed to be proportional to the transport of turbulent kinetic energy, and the diffusion of Reynolds stresses is neglected. Accordingly,

$$\overline{v_i' v_j'} = \frac{2}{3} \delta_{ij} k + \frac{1-\gamma}{c_1} \left(\frac{P_{ij}/\varepsilon - (2/3) \delta_{ij} P/\varepsilon}{1 + (P/\varepsilon - 1)/c_1} \right) \qquad (3.47)$$

where $\gamma \approx 0.6$, and the rest of the notations are the same as in the Reynolds stress equation. Successful application of the algebraic Reynolds stress models can be found in a number of publications [74,81,82]; hence, it is not elaborated herein. But its extension to unsteady turbulent flows remains to be tested. Computational time for using algebraic Reynolds stress models is comparable to the k-ε turbulence models for most of the cases.

Extension of the k-ε turbulence models to unsteady flows has been limited to flows with simple geometries [83] and boundary layer flows. Even for these cases, straight forward extension of the k-ε turbulence models has been more unsuccessful than successful. These model inadequacies motivated a group of researchers to devise a new triple decomposition model of turbulence [84], in which any fluctuating quantity is decomposed into three parts, i.e., time mean quantity, organized oscillations, and random fluctuations. However, this method also remains to be further studied to be useful for engineering calculations.

A successful application of the standard k-ε type turbulence model to unsteady recirculating turbulent flow can be found in Boyle and Golay [85]. Measured velocity field and computed velocity field at 80 sec into transient of the scaled nuclear reactor outlet plenum are shown in Figure 11 [87]. Experimental and computational velocity components, at various locations inside of the plenum chamber, which vary in time are shown in Figure 12 [87]. The computational results compare favorably with experimental data during the flow development period, but the same results begin to diverge from experimental data as steady state is approached.

3.3.2 Large Eddy Simulation (LES) Method

In turbulent flows, instability of mean flow generates large eddies and these large eddies break up into smaller eddies. After many cascade processes, see Figure 13 [86], the fine scale eddies are dissipated by viscous forces. The scale of large scale turbulence, or motion of large eddies, strongly depends on the type of flow and geometry of the flow field; whereas, fine scale turbulence, or motion of fine scale eddies, is almost universal for any turbulent flows. Therefore, fine scale turbulence can be modeled more easily than the large scale turbulence due to its universality. The large eddy simulation (LES) method best utilizes these physical observations. Until now, the LES method has been used for channel flows and axisymmetric annular flows.
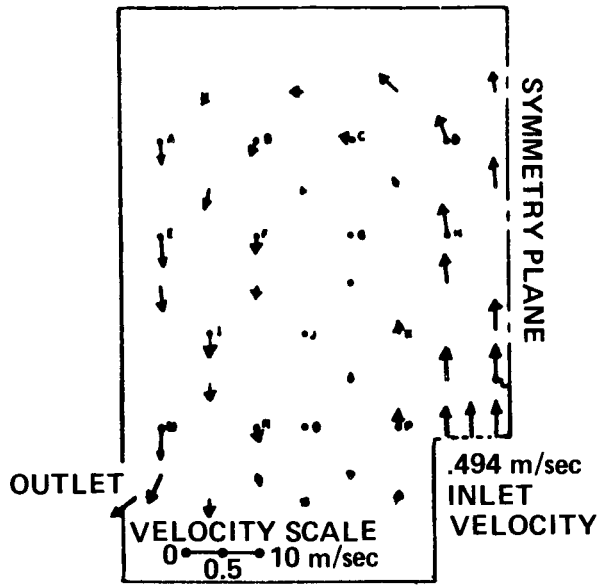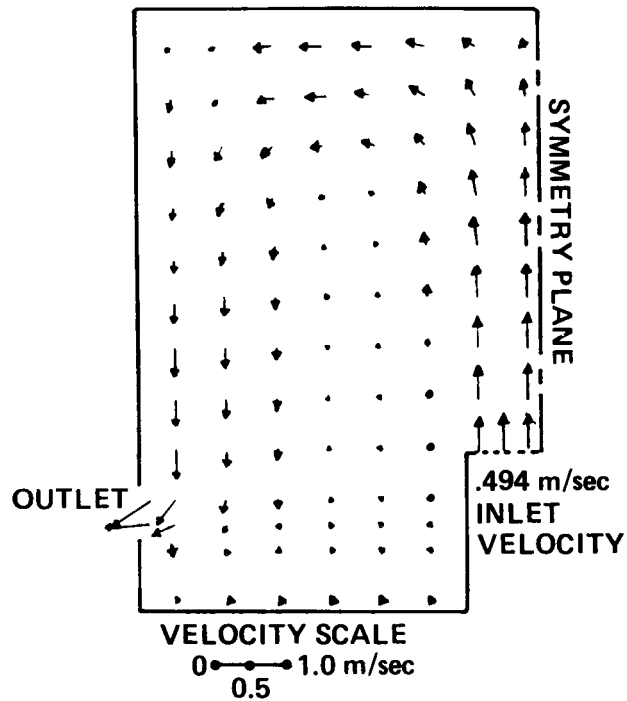
Figure 11. Turbulent recirculating flow in a nuclear reactor outlet plenum [85]. (a) Measure mean velocity profile after 80 sec into transient. (b) Computed mean velocity profile after 80 sec into transient.
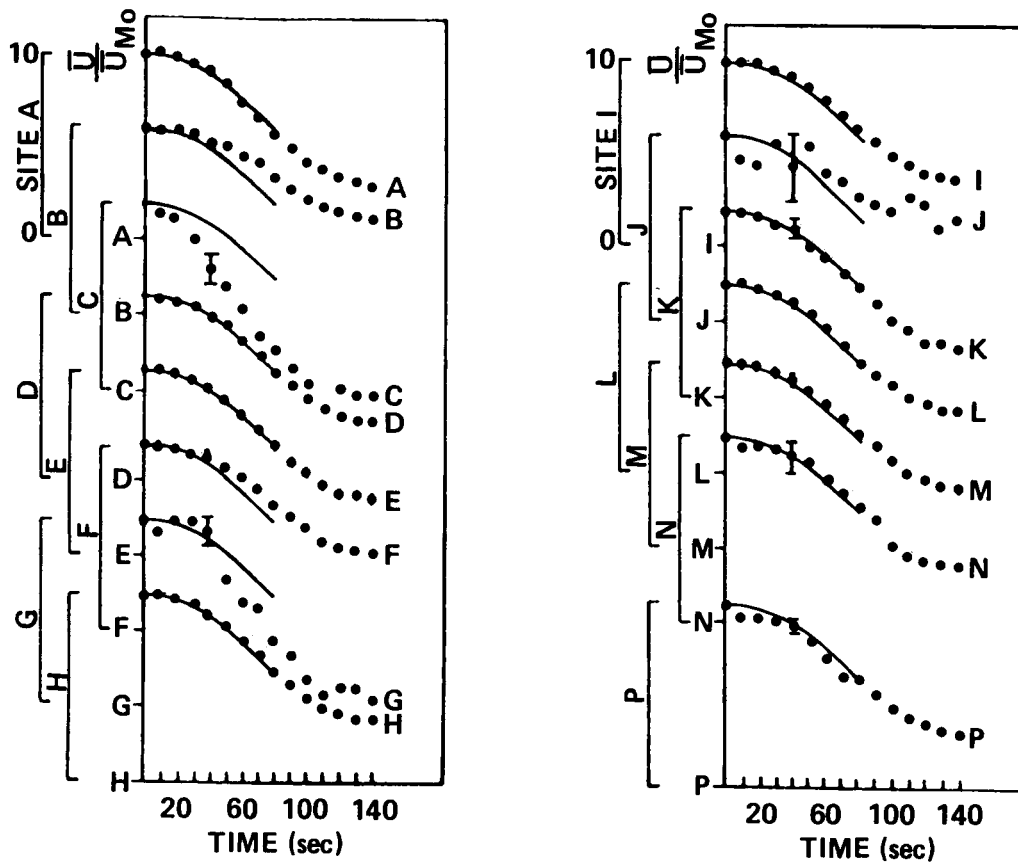
Figure 12. Comparison of measured vertical velocity with computer
velocity [85], a through h in the Figure denotes spatial
locations specified in Figure 10(a).
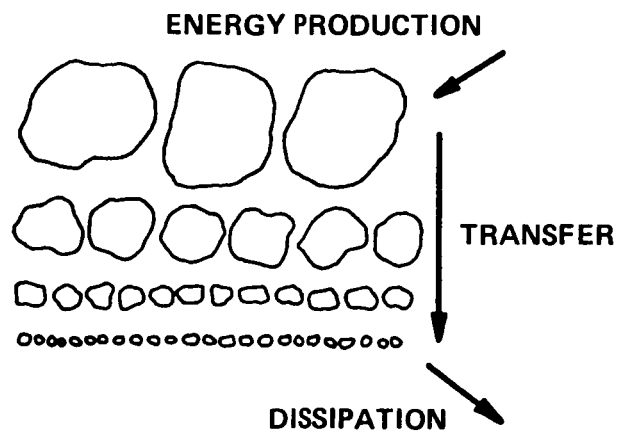
Figure 13. The energy cascade process [86].

In the large eddy simulation method, any flow variable is averaged over a finite volume which is determined by the grid size used in computations. This process is called filtering. Let Ψ be some flow variable, then Ψ can be decomposed as:

$$\Psi = \overline{\Psi} + \Psi'$$ (3.48)

where Ψ' is called the residual field, and $\overline{\Psi}$ is the large scale field defined as:

$$\overline{\Psi}(\underset{\sim}{x},t) = \int_{\Delta V} G(\underset{\sim}{x},\underset{\sim}{x}') \, \Psi(\underset{\sim}{x}',t) \, d\underset{\sim}{x}$$ (3.49)

where $\Delta V = \Delta x_1 \Delta x_2 \Delta x_3$, $\Delta x_k (k=1,2,3)$ is the grid size in the k-th spatial coordinate direction, and the integration is performed over the volume ΔV. The filtering function, $G(\underset{\sim}{x},\underset{\sim}{x}')$, in equation (3.49), was first introduced by Leonard [87] in order to account for nonnegligible variation of large scale motion inside of the averaging volume, ΔV. The filtering function is given as:

$$G(\underset{\sim}{x},\underset{\sim}{x}') = G_1(x_1,x_1') \, G_2(x_2,x_2') \, G_3(x_3,x_3')$$ (3.50)

where $G_i (i=1,2,3)$ is the distribution function. The most frequently used distribution function is the Gaussian distribution function given as:

$$G_i(x_i,x_i') = \sqrt{\frac{6}{\pi}} \frac{1}{\Delta} e^{\{-6(x_i-x_i')^2/\Delta^2\}}$$ (3.51)

where Δ is twice the computational mesh size in x_i-coordinate direction. Many different forms of filtering functions can be used in practice. For example, $G(\underset{\sim}{x},\underset{\sim}{x}') = 1$ was used in the first application of the LES method in Deardroff [88]. A flux form of the Navier-Stokes equation used in LES is given as [88]:

$$\left.\begin{array}{l} \dfrac{\partial v_i}{\partial t} + \dfrac{\partial}{\partial x_j} (v_i v_j) = \dfrac{1}{\rho} \dfrac{\partial P}{\partial x_i} + \nu \nabla^2 v_i \\[2em] \dfrac{\partial \overline{v_j}}{\partial x_j} = 0 \end{array}\right\}$$ (3.52)

Filtering equation (3.52), using any filtering function $G(x,x')$, yields:

34

$$\frac{\partial \overline{v}_i}{\partial t} + \frac{\partial}{\partial x_j}(\overline{v}_i \overline{v}_j) = -\frac{\partial}{\partial x_i}\left(\frac{\overline{P}}{\rho} + \frac{1}{3}\eta_{kk}\right) + \frac{\partial \tau_{ij}}{\partial x_j} + \nu\nabla^2 \overline{v}_i$$

$$\frac{\partial \overline{v}_j}{\partial x_j} = 0 \qquad\qquad\qquad (3.53)$$

where $\overline{v_i v_j} = \overline{\overline{v}_i \overline{v}_j} + \eta_{ij}$, $\eta_{ij} = \overline{v_i'\overline{v}_j} + \overline{\overline{v}_i v_j'} + \overline{v_i' v_j'}$, $\tau_{ij} = -(\eta_{ij} - \eta_{kk}\delta_{ij}/3)$, and δ_{ij} is the Kronecker delta. A subgrid-scale-model (closure model for LES equation) of the residual stress, $\overline{v_i' v_j'}$, due to Deardroff [88] is given by:

$$\lambda_{ij} = \overline{\overline{v}_i \overline{v}_j} - \overline{v}_i \overline{v}_j = 0 \qquad\qquad\qquad (3.54)$$

$$\tau_{ij} = k\left(\frac{\partial \overline{v}_i}{\partial x_j} + \frac{\partial \overline{v}_j}{\partial x_i}\right) \qquad\qquad\qquad (3.55)$$

where $\overline{\overline{v}_i v_j'} = \overline{\overline{v}_j v_i'} = 0$, and c_Δ is a constant to be determined experimentally. Lilly [89] proposed $c_\Delta = 0.17$, Deardorff [88] used $c_\Delta = 0.1$, and Moin and Kim [90] used $c_\Delta = 0.065$. In equation (3.53), $\eta_{kk}\delta_{ij}/3$ has been added to the pressure gradient term to compensate for the same term appearing in the τ_{ij} expression so that equation (3.55) holds when the subscripts i and j are contracted. Consequently η_{kk} in equation (3.53) need to be modeled separately, and Lilly [89] proposed:

$$\frac{1}{3}\overline{v_k' v_k'} = \frac{2}{3}\frac{K^2}{(c_1\Delta)^2} \qquad\qquad\qquad (3.57)$$

where $c_1 = 0.094$.

The governing equation for pressure distribution can be obtained as follows. By letting $\hat{P} = p/\rho + \eta_{kk}/3$ and taking the divergence of the momentum equation, equation (3.53), yields:

$$\nabla^2 \hat{P} = \frac{\partial}{\partial x_i}\left(\frac{\partial \tau_{ij}}{\partial x_j}\right) - \frac{\partial^2}{\partial x_i \partial x_j}(\overline{v}_i \overline{v}_j) \qquad\qquad\qquad (3.58)$$

where dissipation due to molecular viscosity has been neglected and the time derivative term can be dropped out using the conservation of mass condition.

35

Several different methods have been used by different workers [88,91,92] to solve the LES equation, and the form of the LES equations were slightly modified to be suitable for each of the numerical methods used. In Deardorff [88], the classical finite difference method was used to solve the LES equation as given in equation (3.53); in Schumann [91], the control volume finite difference method [90] was used and any time derivative term appearing in the Navier-Stokes equations was filtered over the control volume as before whereas the rest of the terms appearing as fluxes in the control volume finite difference method was filtered over each of the surfaces of the control volume where fluxes are evaluated. In Moin and Kim [92], the pseudo-spectral method [63,64] and the LES equation of the rotational form of the Navier-Stokes equations, i.e., equation (3.23), were used. Particularly in Moin and Kim [92], the LES equation was refined to include the exact treatment of the Leonard's stress, i.e., equation (3.54), and molecular viscosity.

The computational results given in these references [86,88,92] compare excellently with experimental data. But it should be noted that the constant coefficient c_Δ, used in equation (3.56), as proposed by Lilly [89], is larger than twice the value used in Moin and Kim [92]. Hence, the eddy diffusity, which is proportional to the square of c_Δ, used in these calculations for the similar channel flows is quite different. Conceptually, the subgrid-scale-model should not dominate the computational results when fine grids are used for numerical analysis, and the residual stress itself should vanish as computational grid becomes infinitely small. But the afore-mentioned computational results, using practical grid size, showed that the subgrid-scale model is important to render the computational results comparable to experimental data. Therefore, further refinement of the subgrid-scale-model need to be made for the LES method to be applicable to practical engineering calculations.

3.4 Structural Analysis Methods Including Large and/or Permant Deformations

Due to fluidelastic instability, thin cylinders in tube banks may go through large deformations which may cause viscoplastic deformations of the cylinders. There-fore, the structural analysis method to be used for flow-solid interaction of tube banks need to be capable of modeling elastic vibrations as well as large and/or permanent viscoplastic deformations, in order to predict Bauschinger effect, hysteretic effect, and cyclic straining. But to date, no specific numerical structural analysis method designed for this purpose has been developed. Structural analysis methods which can be further developed to meet these requirements are discussed in this section.

Most of the structural analysis methods are based on the finite element displacement method. The finite element system of equations are derived through the minimization of energy functional or derived from the virtual work principle. Elasticity problems are usually described on the frame work of Eulerian coordinate system; and hyperelasticity, large deformations, and viscoplastic deformation problems are usually described on the convected coordinate system in order to account for large displacements. In the methods utilizing the convected coordinate system, the virtual work principle is described on the Lagrangian coordinate system which is updated at each of the solution time levels. The virtual work principle and the minimization of energy functionals are identical for elasticity problems; but the virtual work principle is more convenient for geometrically and/or materially nonlinear problems, since derivation of energy functionals for nonlinear problems can be avoided. In the following discussions, the virtual work principle and the convected coordinate system are used.

For time dependent deformation of structures, consider a point initially at $x_i(i=1,2,3)$ moved to $u_i(1=1,2,3)$ in the same cartesian coordinate system. In Lagrangian formulation, the deformations are described in terms of the convected coordinates $u_i(i=1,2,3)$. The force equilibrium equation, or the momentum equation, for a structural system is given as

$$\sigma_{ij,j} + b_i = 0 \tag{3.59}$$

$$\underset{\sim}{u}(\underset{\sim}{x},t) = \underset{\sim}{u}_o(t) \quad \text{on} \quad \partial\Omega_1 \tag{3.60}$$

$$\sigma_{ij} \, n_j = T_i(t) \quad \text{on} \quad \partial\Omega_2 \tag{3.61}$$

where b_i is the body force; Ω is the structural domain; $\partial\Omega_1$ is the boundary on which the Dirichlet boundary condition is specified; $\partial\Omega_2$ is the boundary on which surface traction is specified; $\partial\Omega_1 \cap \partial\Omega_2$ is a null set, $\partial\Omega_1 \cup \partial\Omega_2 = \partial\Omega$, and $\partial\Omega$ is the entire boundary of the domain; both the surface traction $T_i(t)$ and the prescribed displacements $u_0(t)$ are functions of time in general; and $\underset{\sim}{n}$ is an outward normal vector on the boundary. The inertial force due to acceleration is usually included into the momentum equation as a negative body force. The virtual work statement is given as:

$$\int_\Omega (-\sigma_{ij,j} - b_i) \, \delta u_i \, dx + \int_{\partial\Omega_2} (\sigma_{ij}n_j - T_i) \, \delta u_i \, ds = 0 \tag{3.61}$$

where $\delta u_i(i=1,3)$ is the virtual displacement which satisfies the Dirichlet boundary condition, equation (3.60), on the boundary $\partial\Omega_1$. Integrating by parts the stress term and using the fact that

$$\int_{\partial\Omega_1} \sigma_{ij}n_j \delta u_i dS = 0 \quad ,$$

since $\delta u_i = 0$ on $\partial\Omega_1$ in equation (3.61), yields:

$$\int_\Omega \sigma_{ij} \, \delta u_{i,j} \, d\underset{\sim}{x} - \int_\Omega b_i \, \delta \underset{\sim}{u}_i \, d\underset{\sim}{x} - \int_{\partial\Omega_2} T_i \, \delta u_i \, dS = 0 \tag{3.62}$$

which is the virtual work expression to be used in the finite element method. In finite element analysis, it is more convenient to write the stress tensor, σ_{ij}, and the

strain tensor, ε_{ij}, into column vectors $\underset{\sim}{\sigma}^T = \{\sigma_{xx}, \sigma_{yy}, \sigma_{zz}, \sigma_{xy}, \sigma_{yz}, \sigma_{zx}\}$, and $\underset{\sim}{\varepsilon}^T =$ $\{\varepsilon_{xx}, \varepsilon_{yy}, \varepsilon_{zz}, \gamma_{xy}, \gamma_{yz}, \gamma_{zx}\}$. The shearing strain tensor, $\varepsilon_{ij}(i \neq j)$, is not equal to the engineering shearing strain, $\gamma_{ij}(i \neq j)$, hence adequate modification need to be included in the material property coefficients in the stress-strain relationship. Using the matrix notations, $\sigma_{ij}\delta u_{i,j}$ can be expressed as $\delta \underset{\sim}{\varepsilon}^T \underset{\sim}{\sigma}$. Let

$$\underset{\sim}{u} = \underset{\approx}{N} \, \underset{\sim}{a}$$

$$\underset{\sim}{\varepsilon} = \underset{\approx}{L} \, \underset{\sim}{u} \qquad\qquad (3.63)$$

$$\underset{\sim}{\varepsilon} = \underset{\approx}{B} \, \underset{\sim}{a}$$

where $\underset{\approx}{N}$ is a matrix of interpolating polynomials, $\underset{\sim}{a}$ is the column vector of nodal displacements, $\underset{\approx}{L}$ is a differential operator, and $\underset{\approx}{B} = \underset{\approx}{L}\underset{\approx}{N}$. For geometrically nonlinear problems, $\underset{\approx}{L}$ and $\underset{\approx}{B}$ depend on displacements. Introducing equations (3.63) into equation (3.62) and taking the variation of equation (3.62) with respect to the nodal displacements yields, in matrix notation,

$$\int_\Omega \underset{\approx}{B}^T \, \underset{\sim}{\sigma} \, d\underset{\sim}{x} - \int_\Omega \underset{\approx}{N}^T \, \underset{\sim}{b} \, d\underset{\sim}{x} - \int_{\partial\Omega_2} \underset{\approx}{N}^T \, \underset{\sim}{T} \, dS = 0 \quad . \qquad (3.64)$$

For geometrically and/or materially nonlinear problems, equation (3.64) is not generally satisfied at any computational stage. Hence, writing equation (3.64) in incremental form yields

$$\int_\Omega d\underset{\approx}{B}^T \, \underset{\sim}{\sigma} \, d\underset{\sim}{x} + \int_\Omega \underset{\approx}{B}^T \, d\underset{\sim}{\sigma} + \int_\Omega \underset{\approx}{N}^T \, d\underset{\sim}{b} \, d\underset{\sim}{x} - \int_{\partial\Omega_2} \underset{\approx}{N}^T \, d\underset{\sim}{T} \, dS \qquad (3.65)$$

where $d\underset{\sim}{T} = 0$ if the surface traction is not incremented at any computational stage.

Equation (3.62), or equation (3.65), represents the most general form of the finite element equation for any spatial dimensions; however, its specific forms for different problems and different solution methods are so diverse that they cannot be covered in this review. These different problems include: different strain/stress assumptions; geometrical differences such as one dimensional bars, two dimensional plates, and quasi three dimensional shells, etc.; and the geometrical and/or material nonlinearities. Different solution methods include: interpolation methods such as Lagrangian interpolating polynomials and the Hermite interpolating polynomials; different formulations such as mixed formulation and displacement formulation; and even time integration methods. Only a couple of algorithms that can be extended easily for the flow-solid interaction analysis are covered herein. These are the elasto-viscoplasticity analysis method of Hughes and Taylor [93] and the nonlinear

vibration analysis method, which includes large deformation and elasto-viscoplastic deformations, due to Rodal et al. [99,100].

The most rigorous mathematical treatment of viscoplastic deformation can be found in Hughes and Taylor [93] and Owen and Hinton [94]. In References 93 and 94, a linear strain-displacement relationship has been used and the acceleration force has been neglected, on the assumption that it is negligible compared with forces which cause plastic deformation. Hence, the method is suitable for problems in which only the permanent plastic deformation is important, but not suitable for problems in which the vibrational aspect is as important as the permanent plastic deformations. The general form numerical analysis method for viscoplasticity due to Hughes and Taylor [93] and Owen and Hinton [94] is given below.

In elasto-viscoplastic analysis, it is assumed that the total strain rate, $\underset{\sim}{\varepsilon}$, can be decomposed into an elastic part, $\underset{\sim}{\varepsilon}_e$, and a viscoplastic part, $\underset{\sim}{\varepsilon}_{vp}$, i.e.,

$$\dot{\underset{\sim}{\varepsilon}} = \dot{\underset{\sim}{\varepsilon}}_e + \dot{\underset{\sim}{\varepsilon}}_{vp} \tag{3.66}$$

where the over-dot, ($\dot{}$) notation denotes time rate of change. The viscoplastic strain rate due to Perzyna [95] is given as:

$$\dot{\underset{\sim}{\varepsilon}}_{vp} = \gamma < \phi(F) > \frac{\partial Q}{\partial \underset{\sim}{\sigma}} \tag{3.67}$$

where γ is the fluidity of the plastic flow; $<\phi(F)>$ implies $<\phi(F)> = \phi(F)$ if $F > 0$, and $<\phi(F)> = 0$ if $F < 0$; F is the yield function such as the Huber-von Mises yield function [55], and Q is the plastic potential function. For associated plasticity, F is identical to Q, but different for nonassociated plasticity. The stress rate is related to the elastic strain rate as:

$$\dot{\underset{\sim}{\sigma}} = \underset{\approx}{D} \, \dot{\underset{\sim}{\varepsilon}}_e = \underset{\approx}{D} \, (\dot{\underset{\sim}{\varepsilon}} - \dot{\underset{\sim}{\varepsilon}}_{vp}) \tag{3.68}$$

or, in incremental form,

$$\Delta \underset{\sim}{\sigma}^n = \underset{\approx}{D} (\Delta \underset{\sim}{\varepsilon}^n - \Delta \underset{\sim}{\varepsilon}_{vp}^n) \tag{3.69}$$

where the superscript n denotes the time level $t = t_n$, Δ denotes increment, and the increment is defined for a time interval from t_n to t_{n+1}, i.e., $\Delta t_n = t_{n+1} - t_n$. The viscoplastic strain increment, $\Delta \underset{\sim}{\varepsilon}_{vp}^n$, can be interpolated as

$$\Delta \underset{\sim}{\varepsilon}_{vp}^n = \Delta t_n \{(1-\theta) \, \dot{\underset{\sim}{\varepsilon}}_{vp}^n + \theta \dot{\underset{\sim}{\varepsilon}}_{vp}^{n+1} \} \tag{3.70}$$

where θ is an interpolation parameter such that $\theta = 0$ corresponds to the fully explicit time integration method, $\theta = 1$ corresponds to the fully implicit method, and $\theta = 1/2$ corresponds to the Crank-Nicholson type method. The time integration method for the present elasto-viscoplasticity analysis is unconditionally stable for $\theta \geq 1/2$. As a remark, numerical stability does not imply that convergent solutions can always be obtained for many nonlinear problems. Since the viscoplastic strain rate is a function of stress state, equation (3.70) can be rewritten as

$$\Delta \underset{\sim}{\varepsilon}_{vp}^n = \Delta t_n \, \dot{\underset{\sim}{\varepsilon}}_{vp}^n + \underset{\approx}{c}_n \, \Delta \underset{\sim}{\sigma}^n \qquad (3.71)$$

where $(\dot{\underset{\sim}{\varepsilon}}_{vp}^{n+1} - \dot{\underset{\sim}{\varepsilon}}_{vp}^n) = (\partial \dot{\underset{\sim}{\varepsilon}}_{vp} / \partial \underset{\sim}{\sigma})^n \Delta \underset{\sim}{\sigma}^n$ has been used, and $c_n = \theta \Delta t_n (\partial \dot{\underset{\sim}{\varepsilon}}_{vp} / \partial \underset{\sim}{\sigma})^n$. The incremental strain-incremental displacement relationship can be written as:

$$\Delta \underset{\sim}{\varepsilon}^n = \underset{\approx}{B} \, \Delta \underset{\sim}{a}^n \qquad (3.72)$$

where $\underset{\approx}{B}$ is a constant matrix for infinitesimal strain-displacement relationship. Substituting equations (3.71) and (3.72) into equation (3.69) yields:

$$\Delta \underset{\sim}{\sigma}^n = \hat{\underset{\approx}{D}}^n (\underset{\approx}{B} \, \Delta \underset{\sim}{a}^n - \dot{\underset{\sim}{\varepsilon}}_{vp}^n \, \Delta t_n) \qquad (3.73)$$

where $\hat{\underset{\approx}{D}}^n = (\underset{\approx}{D}^{-1} + \underset{\approx}{C}^n)^{-1}$. Equation (3.73) is the incremental constitutive equation to be used in the incremental virtual work principle, i.e., equation (3.65). For material nonlinearity only, the incremental virtual work equation is given as:

$$\int_\Omega \underset{\approx}{B}^T \, \Delta \underset{\sim}{\sigma}^n \, d\underset{\sim}{x} + \Delta \underset{\sim}{f}^n = 0 \qquad . \qquad (3.74)$$

Inserting equation (3.73) into equation (3.74) yields

$$\int_\Omega \underset{\approx}{B}^T \, \hat{\underset{\approx}{D}}^n \, \underset{\approx}{B} \, \Delta \underset{\sim}{a}^n \, d\underset{\sim}{x} - \int_\Omega \underset{\approx}{B}^T \, \hat{\underset{\approx}{d}}^n \, \dot{\underset{\sim}{\varepsilon}}_{vp}^n \, \Delta t_n \, d\underset{\sim}{x} + \Delta \underset{\sim}{f}^n = 0 \qquad . \qquad (3.75)$$

The incremental displacement, Δa_n is obtained by matrix inversion of equation (3.75) as

$$\Delta \underset{\sim}{a}^n = [\underset{\approx}{K}_T^n]^{-1} \int_\Omega \underset{\approx}{B}^T \, \underset{\approx}{D}^n \, \dot{\underset{\sim}{\varepsilon}}_{vp}^n \, \Delta t_n \, d\underset{\sim}{x} - \Delta \underset{\sim}{f}^n \qquad (3.76)$$

where $\underset{\approx}{K}_T^n = \underset{\approx}{B}^T \, \hat{\underset{\approx}{D}}^n \, \underset{\approx}{B}$ is called the tangential stiffness matrix.

40

In Hughes and Taylor [93], the above methodology was used to solve an elasto-viscoplastic deformation of a thick wall cylinder subjected to constant internal pressure. The physical problem was reduced to a one-dimensional problem by assuming an axisymmetric plane strain state. The physical problem and the computational results are shown in Figure 14.

THICK-WALLED CYLINDER

INTERNAL PRESSURE VS TIME

(a)

— EXACT PLASTICITY SOLUTION [5]

● FINITE ELEMENT RESULTS AT GAUSS POINTS

$a = 1.0$ t -= $t = 10^6$

RESULTS FOR TIME STEPS 2–12 ARE IDENTICAL

(b)
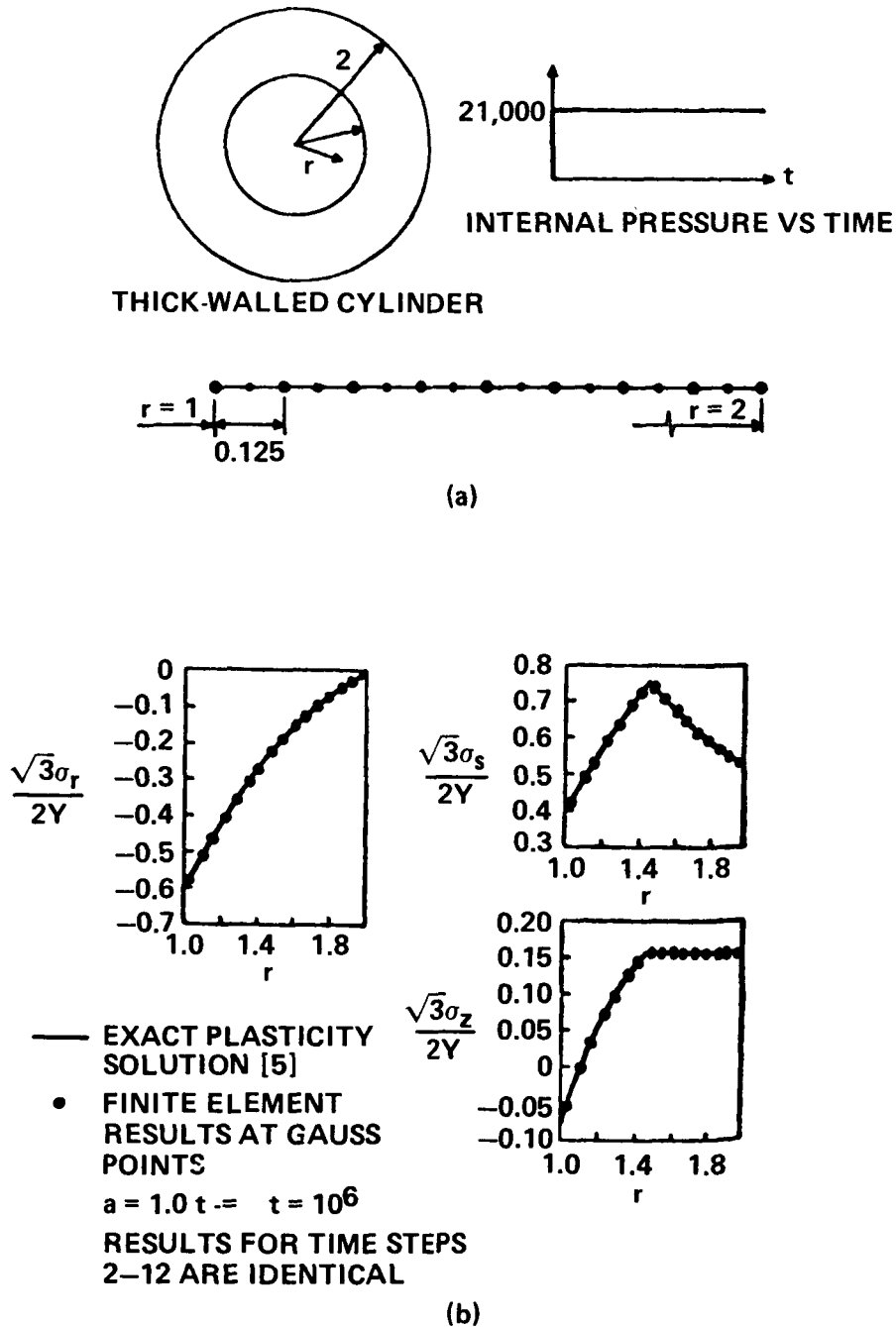
Figure 14. An elasto-viscoplasticity analysis of a thick cylinder subjected to internal pressure [93]. (a) Description of physical problem and a finite element discretization. (b) Comparison with exact plasticity solution.

The numerical analysis method given in equations (3.66) through (3.76) are so general that it can be used for any elasto-viscoplastic problems. Yet, specific forms of strain-displacement relationships for individual problems need to be derived. For flow-solid interaction of tube banks, a general shell element would be preferred.

Refinement of the lasto-viscoplasticity analysis methods in References [93] and [94] can be made in several different ways. These refinements would be: incorporation of temperature dependency of the viscoplastic strain rate into equation (3.67); inclusion of geometrical nonlinearity; inclusion of work hardening into the yield function; and inclusion of the acceleration force term into the governing equation so that Bauschinger effect, hysteretic effect, and cyclic strain hardening can be predicted. Examples of temperature dependent viscoplastic strain rate can be found in References 96 and 97, in which flow formulation was used and the effect of elasticity was completely neglected. Examples of geometrical nonlinearity and work hardening can be found in References 98, 99, and elsewhere.

Rodal et al. [99,100] developed a finite element structural analysis method which includes finite strain, large deformation, and elasto-viscoplasticity so that Bauschinger effect, cyclic straining, and hysteretic effect could be predicted. In this method, all the nonlinearities such as geometrical and material nonlinearities were incorporated into the load vector term so that the contributions of the nonlinearities appear only as modifying forces to the applied load. The structural dynamics equation due to Rodal et al. [99,100] is given as

$$\underset{\approx}{M} \, \dot{\underset{\sim}{a}} + \underset{\approx}{K} \, \underset{\sim}{a} = \underset{\sim}{f} + \underset{\sim}{f}^{n\ell} \qquad\qquad (3.77)$$

where $\underset{\approx}{M}$ is the usual mass matrix, $\underset{\approx}{K}$ is the elastic stiffness matrix, $\underset{\sim}{f}$ is a column vector of externally applied loads, and $\underset{\sim}{f}^{n1}$ is a column vector of modifying loads due to geometrical and material nonlinearities. The computational procedures used in References 99 and 100 are simpler than the one used in References 93 or 94, in which the viscoplasticity has been treated more rigorously. Undoubtedly, the numerical method due to Rodal et al. [99,100] would be adequate for modeling short period vibrations such as those associated with impact problems; but the accuracy of the method as applied to structures vibrating for a longer period of time than the impact duration need to be tested further.

The time dependent elasto-plastic finite element method [57] used in the laminar flow-solid interaction analysis of Donea et al. [51] and Belytschko et al [52,53] are described below together with the Newmark time integration method [101]. The implicit Newmark time integration method is suitable to achieve a rigorous force equilibrium condition in integrating a system of second order ordinary differential equations in the time coordinate direction. But its adequacy for flow-solid interaction has to be tested yet. Elasto-plasticity constitutive equations can be found in a number of publications including References 55 and 102, and are not included herein.

Belytschko and Hsieh [57] developed a time dependent elasto-plasticity finite element method. In this method, infinitesimal strain assumption (a linear strain-displacement relationship) was used and the large dispalcement was taken care of by using the convected coordinate system. The finite element equation used in Reference 57 is given as:

42

$$\int_\Omega \rho \, \underset{\approx}{N}^T \, \underset{\sim}{\ddot{u}} \, d\underset{\sim}{x} + \int_\Omega \underset{\approx}{B}^T \, \underset{\sim}{\sigma} \, d\underset{\sim}{x} = \int_{\partial\Omega_2} \underset{\approx}{N}^T \, \underset{\sim}{T} \, dS \qquad (3.78)$$

which is equivalent to equation (3.64), but the acceleration term appears explicitly. The semi-discretized (fully discretized in spatial coordinates, but left continuous with respect to the time variable) finite element equation becomes

$$\underset{\approx}{M} \, \underset{\sim}{\ddot{a}} - \underset{\approx}{K} \, \underset{\sim}{a} = \underset{\sim}{f} \qquad . \qquad (3.79)$$

In Belytschko and Hsieh [57], the mass matrix was lumped into a diagonal matrix and the elasto-plastic stiffness term was incorporated into the load vector term as a modifying load vector. The resulting system of second order ordinary differential equations was solved explicitly in time. As discussed before, explicit time integration methods are suitable to solve short-period structural responses such as the one for impact problems, or to solve transient problems which asymptotically approach steady state. The force equilibrium condition may not be satisfied rigorously at each time step. The implicit Newmark time integration method which can satisfy force equilibrium condition more rigorously is briefly described below.

In the Newmark time integration method [101], the displacement vector in equation (3.79), which is a continuous function of time, is expanded into a parametric series form such that

$$\underset{\sim}{\ddot{a}}^{n+1} = c_0(\underset{\sim}{a}^{n+1} - \underset{\sim}{a}^n) - c_1 \, \underset{\sim}{\dot{a}}^n - c_2 \underset{\sim}{\ddot{a}}^n$$

$$\underset{\sim}{\dot{a}}^{n+1} = \underset{\sim}{\dot{a}}^n + [(1 - \bar{\alpha}) \, \underset{\sim}{\ddot{a}}^n + \bar{\alpha} \, \underset{\sim}{\ddot{a}}^{n+1}] \, \Delta t_n \qquad (3.80)$$

$$\underset{\sim}{a}^{n+1} = \underset{\sim}{a}^n + \underset{\sim}{\dot{a}}^n \, \Delta t_n + [(0.5 - \bar{\gamma}) \, \underset{\sim}{\ddot{a}}^n + \gamma \, \underset{\sim}{\ddot{a}}^{n+1}] \qquad ,$$

where

$$c_0 = 1/[\bar{\gamma}(\Delta t_n)^2]$$

$$c_1 = 1/(\bar{\gamma} \, \Delta t_n)$$

$$c_2 = 1/2\bar{\gamma} - 1$$

and α and γ are constant such that $(\alpha,\gamma) = (1/2,1/4)$ corresponds to the unconditionally stable, constant-average-acceleration time integration method. Substituting equations (3.80) into equation (3.79) yields

$$(c_0 \underset{\approx}{M} + \underset{\approx}{K}) \, \underset{\sim}{a}^{n+1} = c_0 \underset{\approx}{M} \, [\underset{\sim}{a}^n + (c_1/c_0) \, \dot{\underset{\sim}{a}}^n + (c_2/c_0) \, \ddot{\underset{\sim}{a}}^n] + \underset{\sim}{f} \qquad (3.81)$$

which can be solved for displacements for each new time-level.

3.5 Numerical Solutions of Flows Through a Nest of Cylinders

Only very recently, a group of researchers began to numerically model the fluid flow through tube banks. The recent developments of flow analysis method for tube banks are discussed in this section. These are: control volume finite difference analyses due to Singhal et al. [44], Wambsganss et al. [103], and Sha and Yang [104]; two-dimensional finite element analysis due to Zienkiewicz et al. [105]; and body fitted grid finite difference analyses due to Kwak and Chang [106], Chang and Kwak [107], and Rogers et al. [108]. In all of the above studies, the flow fields were assumed to be steady and the viscosity is constant.

3.5.1 Control Volume Finite Difference Analyses of Steady Laminar Flows Through Tube Banks

For tube banks with a large number of cylinders, detailed numerical modeling of the flow field is prohibited due to the present computer capability including available memory and computational speed. Approximate numerical analysis methods based on the concept of flow through porous media were proposed by Sha et al. [104], Wambsganss et al. [103], and Singhal et al. [44]. In these methods, the flow domain is discretized into a number of cells where each cell contains several cylinders (Fig. 15). Then the resistance of each cell to fluid flow is represented by volume porosity (fraction of volume occupied by the fluid in the cell) and surface permeability (fraction of open projected flow area in the direction of fluid flow in the cell). The governing equations are the same Navier-Stokes equations, but any volumetric quanquantity needs to be multiplied by the volume porosity; and each velocity component, by the surface permeability in the direction of each velocity component. The flow field shown in Figure 8 [44] was obtained by solving the flow equations for porous media using the control volume finite difference method [90].

In the fluidelastic instability analysis of Wambsganss et al. [103], the computed flow velocity normal to the cylinder walls was taken as reference velocity for predicting the fluidelastic instability using the instability diagram shown in Figure 4. The validity of these methods remains in question; since fluidelastic instability is caused primarily by flow-solid interaction, and in most of the cases, the most serious fluidelastic instability is confined to the flow inlet region of tube banks according to experimental observations.

More recently, a new computational method, called the control-volume based finite elements, was developed by Baliza and Patankar [116], Prakash and Patankar [117], and Prakash [118] among many others. The method utilizes isoparametric finite elements to discretize the domain and to interpolate the solution vectors. The discrete system of equations is derived by considering the flux through the element sides as in the control-volume based finite difference method. On the other hand, in the standard finite element methods, the discrete system of equations are derived using the method of weighted residuals (MWR) to be introduced in the following section. The mathematical foundations of the two different methods are quite different; and consequently, the final discrete systems of equations are also quite different.

44
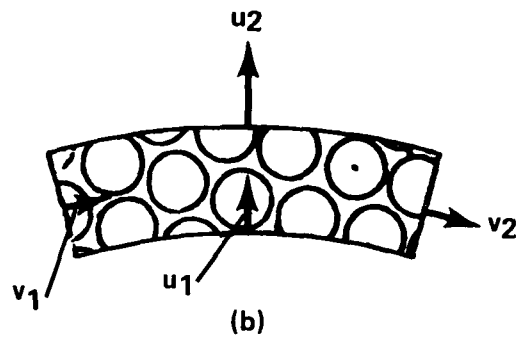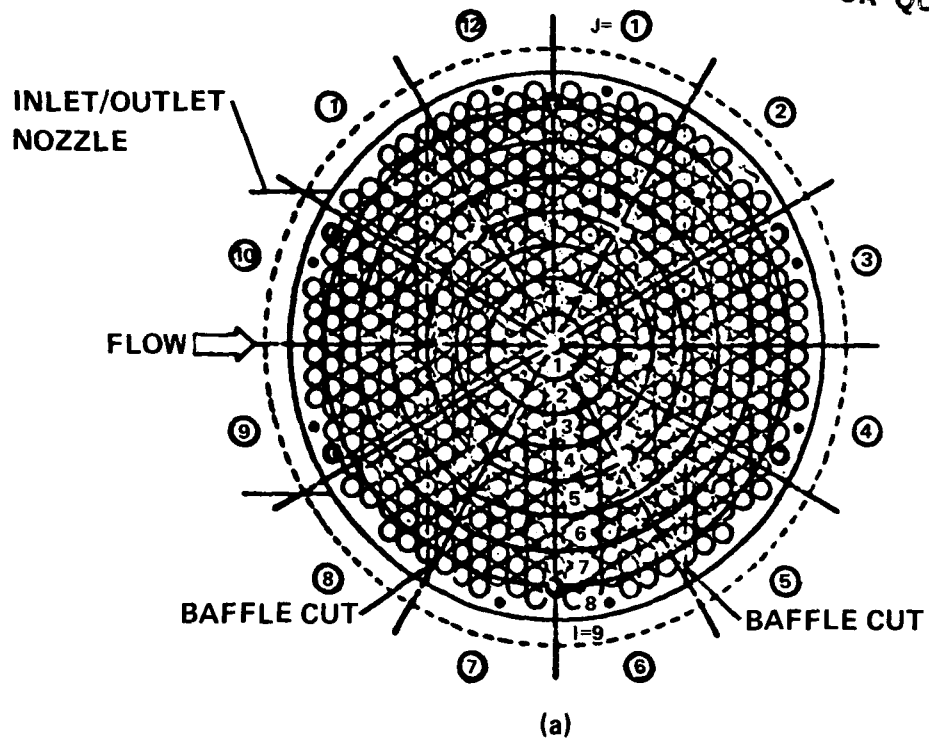
Figure 15. Control volume finite difference analysis of flow through
a porous media [103]. (a) Discretization of a tube bank.
(b) Configuration of a cell.

Until now, the control-volume based finite element method utilized only the linear iso-
parametric elements. In this case, the curved geometry is approximated by straight
lines connecting the nodal points. On the other hand, most of the finite element
methods for structural analysis utilizes quadratic or higher order elements to best
approximate the geometry as well as solution vectors. Use of the control-volume based
finite element method for flow-solid interaction analysis in the future remains as an
open question.

3.5.2 Finite Element Analysis of Steady Two-Dimensional Laminar Flows Through Tube Banks

The finite element method has certain advantages over the finite difference method. These advantages are: capability to include various types of boundary conditions more naturally and rigorously in the formulation; capability to show convergent nature of the method mathematically; and capability to model complicated domains more precisely than the finite difference method.

Application of the finite element method for flows has shorter history than the finite difference method, and the finite element method is still in its early development stage as far as application to fluid flows is concerned. Much of the development time for the finite element method for flows has been spent in overcoming numerical instability arising from convection in high Reynolds number flows. But with the recent development of the Petrov-Galerkin method [109] for convection dominated flows, more rapid development of the method for flows is expected in the near future. The Petrov-Galerkin method and its application to two-dimensional steady laminar flows through tube banks are discussed in this section.

The Bubnov-Galerkin method [109] (in which test functions are selected from the same space as the trial functions) yields exactly the same discrete equation as the central differencing finite difference method for one-dimensional problems discretized using linear elements. As a remark, for most of the cases, the discrete equations obtained through the two different methods are quite different. For a long time, it was believed that the Bubnov-Galerkin method (or equivalently, the central differencing scheme) is the most accurate discrete representation of the continuous differential equations. But, Brooks and Hughes [109] showed that: the Bubnov-Galerkin method underestimates the numerical diffusion; the conventional Petrov-Galerkin method (or equivalently, the backward differencing scheme) overestimates the numerical diffusion; and the optimal Petrov-Galerkin Method (this should be considered as the consistent Petrov-Galerkin method when source terms exist in the differential equation) yields the most accurate numerical results. A finite element solution of one-dimensional convection-diffusion equation of the form:

$$v \frac{\partial T}{\partial x} - k_0 \frac{\partial^2 T}{\partial x^2} = 0 \qquad \text{in} \quad x \varepsilon (0,1) \tag{3.82}$$

with boundary conditions $T(0) = 0$ and $T(1) = 1$, is shown in Figure 16, where T is the temperature. The basis of test functions for the consistent Petrov-Galerkin method is given as [105]

$$\phi_i^*(x) = \phi_i(x) + \frac{\partial \phi_i}{\partial x} v k_0''/|v|^2 \quad , \quad i = 1, N_e \tag{3.83}$$

$$k_0'' = \alpha |v| h/m \tag{3.84}$$
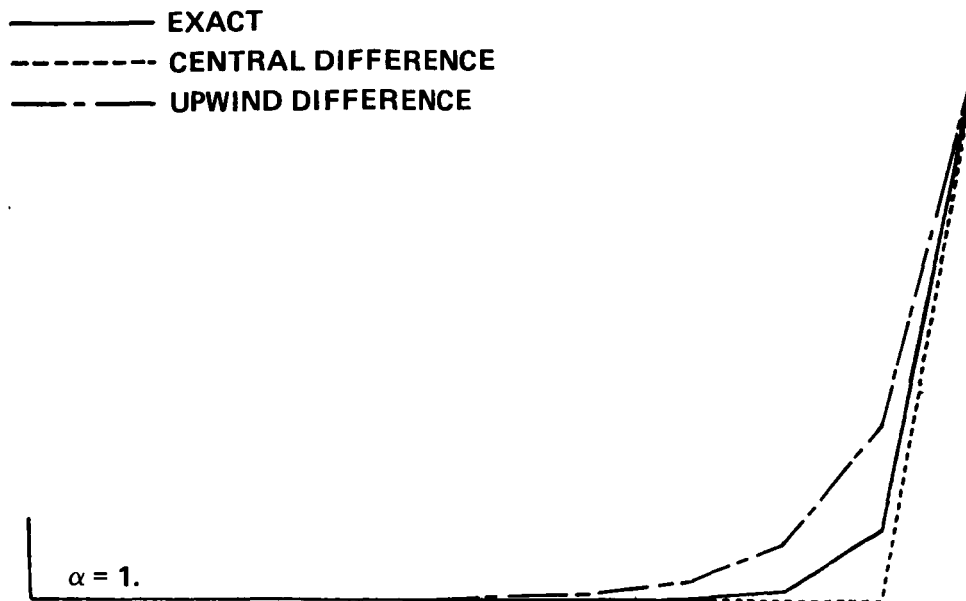
Figure 16. A finite element solution of one-dimensional
convection-diffusion problem.

where $\alpha = \coth(P_e/2) - 2/P_e$, $P_e = |v| h/k$ is the grid Peclet number, v is the convection velocity, $\phi_i(x)$ is the shape function, m = 2 for linear elements, and N_e is the number of nodes in an element. This method naturally extends to two-dimensional flows as shown in the two-dimensional flows through tube banks. Extension of the method to three-dimensional cases was suggested to be the same [105].

For a two-dimensional case, the basis of the test fucntions of the consistent Petrov-Galerkin method is given as [105]:

$$\phi_i^*(\underset{\sim}{x}) = \phi_i^*(\underset{\sim}{x}) + \frac{\partial \phi_i}{\partial x_\ell} v_\ell k_0'' / |v|^2 \quad , \qquad \ell = 1,2 \qquad (3.85)$$

where $\underset{\sim}{x}^T = (x,y)$, k_0'' is the same as in equation (3.84) but $|v| = (v_1^2 + v_2^2)^{1/2}$ at each of the Gauss points used in numerical integration, and h is the length scale of the element.

The finite element equation for Navier-Stokes equations is obtained by the method of weighted residuals. In the method: the flow domain is discretized into a number of elements; the Navier-Stokes equations are multiplied by the test functiqn; the second order diffusion term is integrated by parts; continuous variables are interpolated using the nodal values of the variables and interpolating polynomials; the resulting equations are integrated over each element using the Gauss numerical quadrature to obtain element system of equations; and the element system of equations are assembled together to obtain a global system of equations. A standard finite element system of equations for an element is given in the following.

$$\begin{bmatrix} \underset{\approx}{C}(\underset{\sim}{v}) & \underset{\approx}{0} \\ \underset{\approx}{0} & \underset{\approx}{C}(\underset{\sim}{v}) \end{bmatrix} \begin{Bmatrix} \underset{\sim}{v}_1 \\ \underset{\sim}{v}_2 \end{Bmatrix} + \begin{bmatrix} \underset{\approx}{Q}_1 \\ \underset{\approx}{Q}_2 \end{bmatrix} \{\underset{\sim}{P}\} + \begin{bmatrix} 2\underset{\approx}{K}_{11}+\underset{\approx}{K}_{22} & \underset{\approx}{K}_{12} \\ \underset{\approx}{K}_{21} & 2\underset{\approx}{K}_{22}+\underset{\approx}{K}_{11} \end{bmatrix} \begin{Bmatrix} \underset{\sim}{v}_1 \\ \underset{\sim}{v}_2 \end{Bmatrix} = \begin{Bmatrix} \underset{\sim}{f}_1 \\ \underset{\sim}{f}_2 \end{Bmatrix} \qquad (3.86)$$

$$[\underset{\approx}{Q}_1{}^T \ \underset{\approx}{Q}_2{}^T] \begin{Bmatrix} \underset{\sim}{v}_1 \\ \underset{\sim}{v}_2 \end{Bmatrix} = \{\underset{\sim}{0}\} \qquad (3.87)$$

where

$$\underset{\approx}{C}(\underset{\sim}{v}) = \int \rho v_{1k}\phi_k\phi_i{}^*\phi_{j,x}d\underset{\sim}{x} + \int \rho v_{2k}\phi_k\phi_i{}^*\phi_{j,y}\,d\underset{\sim}{x}$$

$$\underset{\approx}{Q}_1 = \int -\phi_{i}^*{}_{,x}\,\psi_n\,d\underset{\sim}{x}$$

$$\underset{\approx}{Q}_2 = \int -\phi_{i}^*{}_{,j}\,\psi_n\,d\underset{\sim}{x}$$

$$\underset{\approx}{K}_{11} = \int \mu\,\phi_{i}^*{}_{,x}\,\phi_{j,x}\,d\underset{\sim}{x} \qquad\qquad (3.88)$$

$$\underset{\approx}{K}_{22} = \int \mu\,\phi_{i}^*{}_{,y}\,\phi_{j,y}\,d\underset{\sim}{x}$$

$$\underset{\approx}{K}_{12} = \int \mu\,\phi_{i}^*{}_{,y}\,\phi_{j,x}\,d\underset{\sim}{x}$$

$$\underset{\approx}{K}_{21} = \int \mu\,\phi_{i}^*{}_{,x}\,\phi_{j,y}\,d\underset{\sim}{x}$$

In equation (3.88), $i = 1, N_e$; $j = 1, N_e$; $k = 1, N_e$; N_e is the number of velocity nodes in an element; $n = 1, N_p$, N_p is the number of pressure nodes in an element, integration is performed over each element, and $\phi_{i,x}$ denotes $\partial\phi_i/\partial x$, etc.

In practice, the penalty finite element method [119] has been used quite frequently for flow problems (or more frequently for some problems such as polymer extrusion problems [110]). In the penalty method, the unknown pressure is pre-eliminated from the Navier-Stokes equations. The pressure field solution can be obtained in the post process if necessary. The laminar flow through tube banks shown in this section was also solved using the penalty method. To eliminate the pressure variable, we set:

$$\underset{\sim}{\nabla} \cdot \underset{\sim}{v} = P/\alpha_p \qquad\qquad (3.89)$$

where p is the pressure, and α_p is the penalty parameter. As α_p approaches infinity, $\underset{\sim}{\nabla} \cdot \underset{\sim}{v} \approx 0$ and, hence, the continuity condition is satisfied approximately. In these computations, α_p is taken to be 10^7 through 10^{10} times the molecular viscosity to avoid ill-conditioned system of equations. Finite element discretization of equation (3.89) yields

$$[\underset{\approx}{Q}_1^T \quad \underset{\approx}{Q}_2^T] \left\{ \begin{array}{c} \underset{\sim}{v}_1 \\ \underset{\sim}{v}_2 \end{array} \right\} = \frac{1}{\alpha_p} \underset{\approx}{C} \underset{\sim}{p} \tag{3.90}$$

where $\underset{\approx}{Q}_1$ and $\underset{\approx}{Q}_2$ are the same as in equation (3.88), $\underset{\approx}{C} = \int \psi_\ell \psi_n dx$, $\ell = (1, N_p)$, $n = (1, N_p)$, and N_p is the number of pressure nodes in an element as before. Solving for pressure, p, in equation (3.90) and substituting the result into equation (3.86) yields penalized discrete Navier-Stokes equation to be solved for nodal velocities only. The penalized discrete Navier-Stokes equations are given by

$$\begin{bmatrix} \underset{\approx}{C} & \underset{\approx}{O} \\ \underset{\approx}{O} & \underset{\approx}{C} \end{bmatrix} \left\{ \begin{array}{c} \underset{\sim}{v}_1 \\ \underset{\sim}{v}_2 \end{array} \right\} + \alpha_p \begin{bmatrix} \underset{\approx}{Q}_1 \\ \underset{\approx}{Q}_2 \end{bmatrix} \underset{\approx}{C}^{-1} [\underset{\approx}{Q}_1 \quad \underset{\approx}{Q}_2] \left\{ \begin{array}{c} \underset{\sim}{v}_1 \\ \underset{\sim}{v}_2 \end{array} \right\} + \begin{bmatrix} 2\underset{\approx}{K}_{11} + \underset{\approx}{K}_{22} & \underset{\approx}{K}_{12} \\ \underset{\approx}{K}_{21} & 2\underset{\approx}{K}_{22} + \underset{\approx}{K}_{11} \end{bmatrix} \left\{ \begin{array}{c} \underset{\sim}{v}_1 \\ \underset{\sim}{v}_2 \end{array} \right\} = \left\{ \begin{array}{c} \underset{\sim}{f}_1 \\ \underset{\sim}{f}_2 \end{array} \right\} \tag{3.91}$$

Equation (3.91) is ($2N_e$ by $2N_e$) system of equations, and the necessity for solving the conservation of mass equation and the pressure variable has been eliminated. If desired, the pressure field can be recovered by solving equation (3.90) in the post process. One advantage of the penalty method is that the number of unknowns are reduced so that a slight computational efficiency is achieved. But Zienkiewicz [110] has pointed out that solving the standard discrete Navier-Stokes equations can achieve comparable computational efficiency if the frontal solution technique [111] is used and the pressure variables are eliminated at element levels. But in this case, the pressure needs to be discontinuous across element interfaces. The standard solution method would be preferred in the flow-solid interaction analysis since the pressure solution is required for most of the cases. A Petrov-Galerkin finite element solution of two-dimensional steady laminar flow through a tube bank is shown in Figure 17, where the Reynolds number is 500.

Much progress for the Petrov-Galerkin type analysis methods has been made recently for unsteady two-dimensional flows. Among these are: the Taylor-Galerkin method due to Zienkiewicz et al. [105], Donea [112], Lohner et al. [113], and Donea et al. [114], in which Taylor series expansion of the time derivative term is made prior to the spatial discretization, and the Taylor series expanded Navier-Stokes equations are solved by the Bubnov-Galerkin method; and direct extension of the Petrov-Galerkin method for the two-dimensional steady flows into unsteady two-dimensional flows by considering the time-coordinate as an extra spatial coordinate due to Yu and Heinrich [105]. It is believed that most of the upwinding techniques for two-dimensional unsteady flows can be extended to three-dimensional unsteady flows.

(a)

(b)

(c)
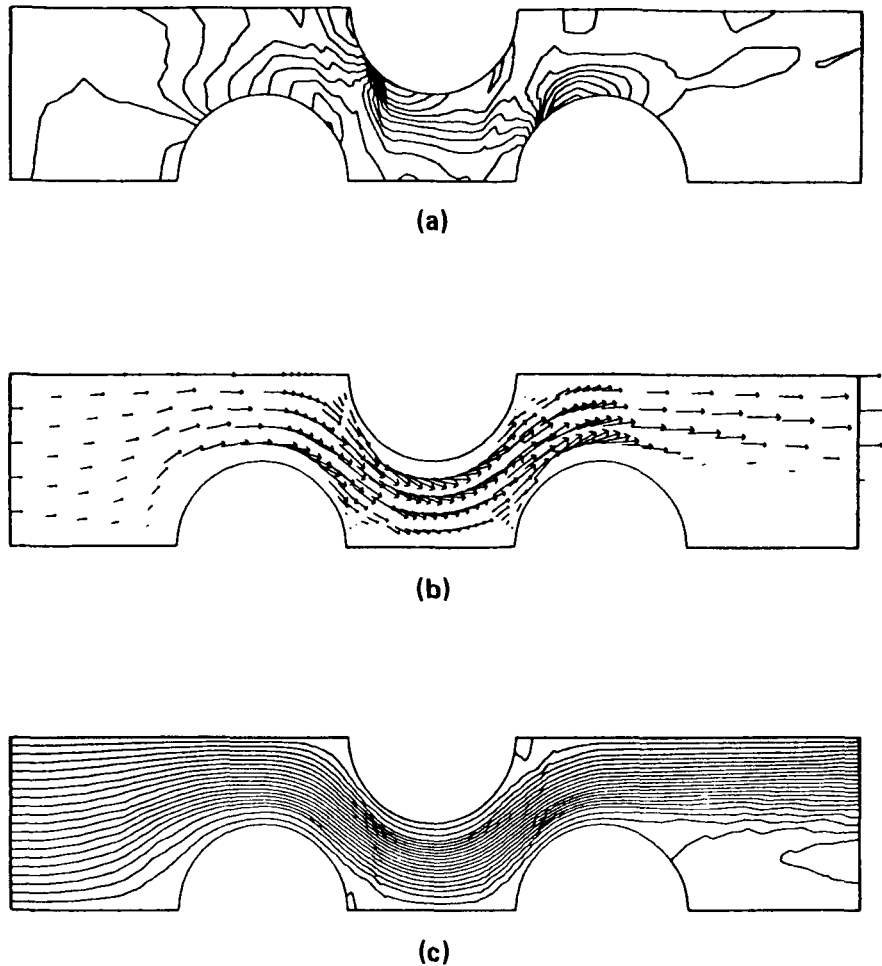
Figure 17.   A Petrov-Galerkin finite element solution of a two-dimensional
steady laminar flow through a tube bank.   (a) Pressure contour
lines.   (b) Velocity vectors.   (c) Stream lines.

Finite element computations of turbulent, separated flows also begin to appear
in the literature.   Among these are Taylor et al. [122], Smith [123], and Benim and
Zinser [124].   In these papers, the standard k-ε turbulence model for high Reynolds
number flows has been used.   In Taylor et al. [122], the flow domain was discretized
using quadratic quadrilateral isoparametric elements as shown in Figure 18a.   The
numerically obtained mean velocity and the turbulence intensity profiles are compared
with experimental data [125] as well as the finite difference solutions [125] in Figures
18b and 18c.   It can be seen that both the finite element method and the finite
difference method predict the mean velocity profile accurately; however, it can also
be seen that the finite element method predicts the turbulence intensity profile better
than the finite difference method for this particular case.

The boundary element method, which has been tested for incompressible laminar
flows [127], also exists.   In this method, the residual function, defined in the same
way as in the finite element methods, is weighted against the test function and inte-
grated over the domain.   But in this method, the test fucntion is the particular solu-
tion of the governing differential equation, and hence the domain integration is reduced
into a boundary integration for Laplace's equation.   But still one needs to integrate

(a)

(b)

(c)
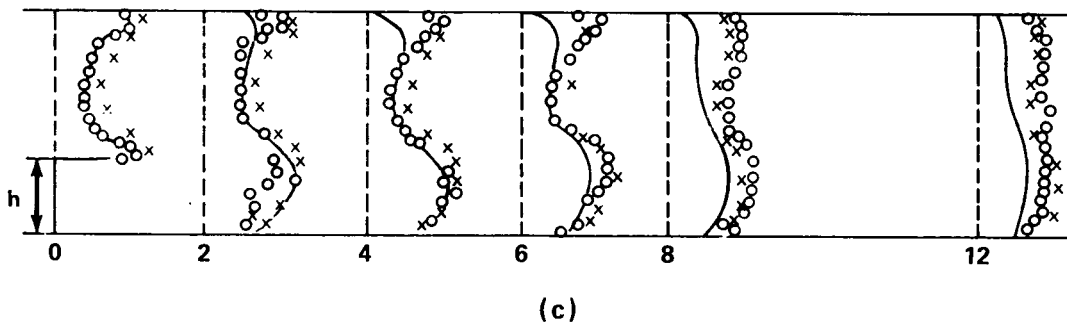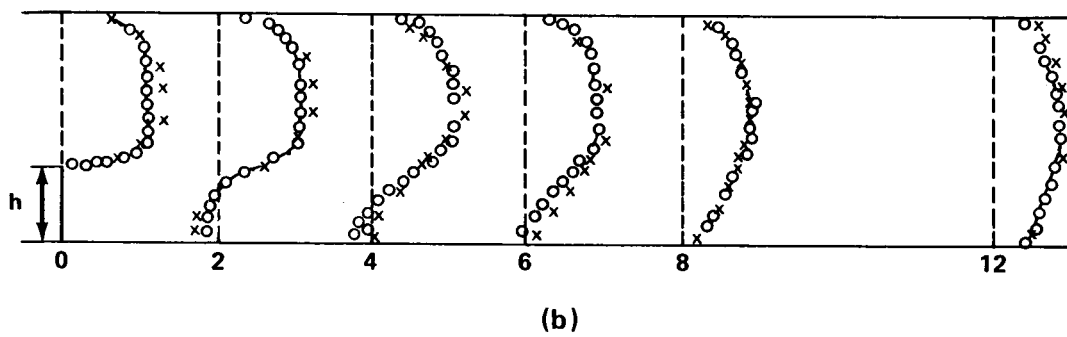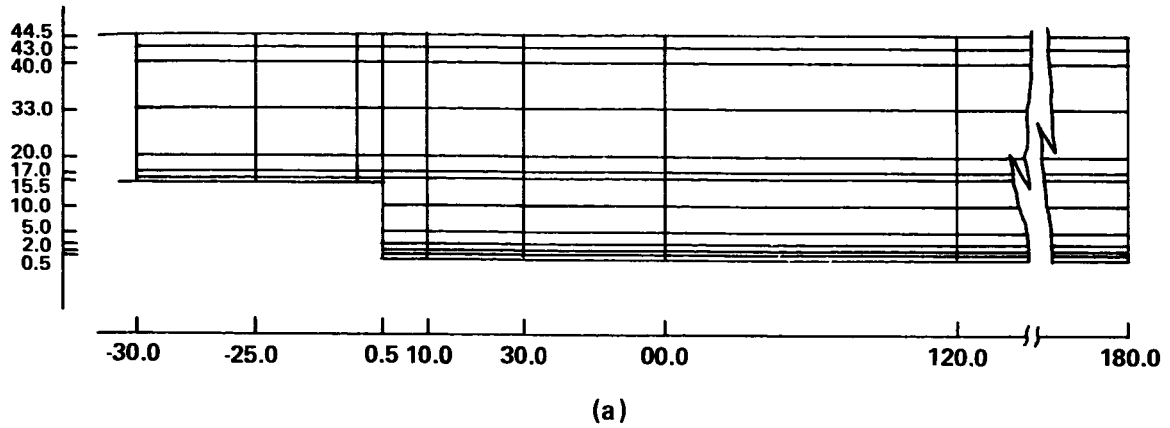
o: EXPERIMENTAL DATA [125], x: FINITE ELEMENT COMPUTATIONAL RESULTS, - — :
FINITE DIFFERENCE SOLUTION

Figure 18.   Flow over a backward-facing step.   (a) Finite element
discretization.   (b) Velocity profile.   (c) Turbulent
kinetic energy profile.

over the domain for Poisson type equations. Originally, the method was applicable only when the particular solution for the governing differential equation is available. For nonlinear problems, the nonlinear terms can be considered as forcing functions in the iterative solution procedure. The method is particularly suitable for problems exhibiting singularities as those associated with fracture mechanics. But the use of the method for turbulent flows is not certain, not to mention the flow-solid interactions.

3.5.3 Body-Fitted Grid Finite-Difference Analysis of Steady Flows Through Tube Banks

In the body-fitted grid finite-difference method, the flow domain is mapped onto an orthogonal computational grid; the flow equations on the computational grid are obtained by transforming the conservation of mass equation, the Navier-Stokes equations, and the energy equation using the coordinate transformation relationship. The resulting system of partial differential equations are solved on the computational grid system.

If the physical flow domain is complicated or highly curved, then the numerical results may not be accurate due to large truncation error involved in the grid transformation relationship. This difficulty was overcome in Kwak and Chang [106] and Chang and Kwak [107] by dividing the flow domain into several sub-domains which overlap at the interface regions. Thus, grid transformation error can be reduced and slight computational efficiency can be achieved by reducing the size of the system of equations to be solved. The body-fitted grid finite-difference method proved to be quite successful for laminar flows, but its extension to turbulent flows is not so obvious as yet. It may be expected that the truncation error in grid transformation may accumulate in an iterative solution procedure of coupled flow and turbulence equations so that the computational results may not be so accurate. Success of the body-fitted grid finite-difference method for complicated turbulent flows may depend on overcoming the truncation error, one method for doing so is the sub-domain method [106,107].

In order to achieve further computational efficiency, a pseudocompressibility method was used in Kwak and Chang [106], Chang and Kwak [107], and Rogers et al. [108], so that a time dependent solution method can be used to obtain a steady state solution. It was shown in References 106, 107, and 108 that the pseudocompressibility method takes less computational time than solving the steady state Navier-Stokes equations directly. Numerically solved grids and flow fields through a cylinder and two rows of cylinders, using the above described method, are shown in Figure 19 [108].

The body-fitted grid finite-difference method is also intended to be further developed for flow-solid interaction analysis of tube banks [106,107,108].

IV. CONCLUSIONS AND RECOMMENDATIONS

This report provides a review of various methods used for design of tube banks as well as computational methods to analyze flow-solid interactions of tube banks subjected to cross flows.

Some conclusions can be made regarding the present state of understanding of the flow field in tube banks and the flow-solid interactions in such tube banks. These are listed below.
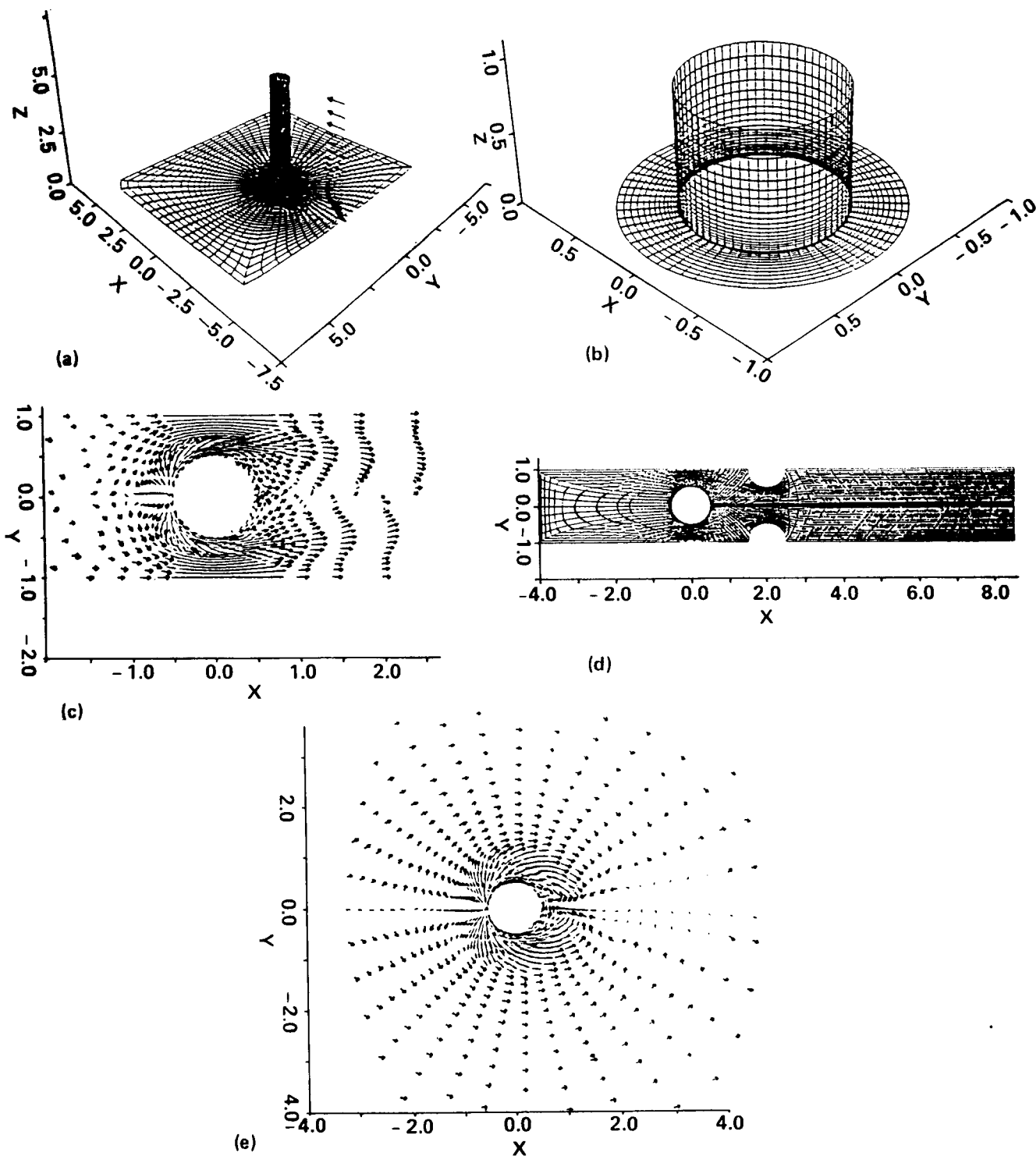
Figure 19. INS3D computation of flow through cylinders. (a) Grid for a single
post on a flat plate. (b) Grid spacing near post-plate junction for a single
post. (c) Velocity vectors for multiple post in z/d = 0.01 plane.
(d) Grid for calculating flow around two rows of cylinders.
(e) Velocity vectors for single post in z/D = 0.01 plane.

1) No major experiment has ever been made for the flow field in the region between tube banks and all the understanding of the flow field depends on conjectures by researchers in this area.

2) Analytical models for flow-solid interaction in tube banks are based on too many restricting assumptions so that these analytical models cannot fully describe the practical problems of interest. Consequently, practical design of tube banks mostly depend on experimental data.

3) Most of the analytical models use the Euler beam equation to represent thin cylinders. The validity of modeling thin cylinders by the Euler beam equation need to be studied further if these models are going to be extended to include large deformations and material nonlinearity.

4) The mathematical model developed by Chen [45] is one of the most complete models relating to this subject, in the sense that it includes multiple number of vibration inducing mechanisms. Many of the coefficients, such as the fluidelastic stiffness coefficients used in the model, need to be supplied by experiments or by computational fluid dynamics as suggested by Chen [45]. But the model can predict only weakly coupled flow-solid interactions. Its usefulness for predicting failure mechanisms such as cyclic straining or hysteretic effects is limited in its present form because of the reasons stated in (3).

5) Detailed numerical modeling of the flow field in the region between tube banks has just begun and the numerical solutions obtained until now are for steady, constant-viscosity flows only.

Solving flow-solid interaction problems requires, in general, capabilities to solve fluid flow problems, structural dynamics problems, and coupling the flow-structure interface conditions. Therefore, the state of development for turbulence models, numerical methods such as the finite element method and the finite difference method, nonlinear structural analysis methods, and existing analytical methods applicable to laminar as well as to turbulent flow-solid interactions have been included in the discussions in order to evaluate the possibility of initiating a development of major numerical analysis method for cross flows.

It was found that the existing numerical analysis methods for flow-solid interactions are designed for specific problems of each researcher's interest. At this time, it is not known whether these methods can be naturally extended to flow-solid interactions for a nest of cylinders subjected to turbulent flow at high Reynolds numbers.

The development stage, advantages, and disadvantages of the various numerical methods discussed in this report are summarized in Table 4 as they are related to the flow-solid interaction analysis.

Based on these observations, some recommendations can be made. These are listed below.

1) Presently, most of the structural analyses have been based on the finite element method. Recent developments in the Petrov-Galerkin finite element method enables the method to be applciable to high Reynolds number flows which in the past had been solved mostly by the finite difference method. It is, therefore, recommended that the use of the finite element method for flow-solid interaction analysis in tube banks be pursued further.

TABLE 4. COMPARISON OF DIFFERENT NUMERICAL METHODS FOR THE NUMERICAL ANALYSIS OF FLOW-SOLID INTERACTIONS

(Smaller number denotes higher rating)

	CV-FDM[1]	BFG-FDM[2]	CV-FEM[3]	FEM[4]	BEM[5]	FDM[6]
Capability to handle nonlinear equations	2	3	2	1	4	1
Capability to handle complicated geometry	3	3	3	2	1	3
Number of grids required	3	3	3	2	1	3
Experience gained for turbulent flow analysis	1	2	3	2	NI[7]	1
Experience gained for structural analysis	NI	NI	NI	1	2	2
Experience gained for flow-solid interaction	NI	NI	NI	1	NI	2
Computer time to solve the same turbulent flows	1	1	2	3	NI	1
Computer time to solve the same nonlinear structural problems	NI	NI	NI	1	2	2

1. CV-FDM — Control-Volume Based Finite-Difference Method
2. BFG-FDM — Body-Fitted Grid Finite Difference Method
3. CV-FEM — Control-Volume Based Finite Element Method
4. FEM — Finite Element Method
5. BEM — Boundary Element Method
6. FDM — Finite Difference Model
7. NI — No Information Available.

2) One of the best performing elements for shell structures are the Ahmad element [55] and the semiloop element [126]. Use of these elements for geometrically and/or materially nonlinear structures has been reported elsewhere, including References 55 and 126. But use of these elements for vibration problems which require rigorous mathematical modeling of elasto-viscoplasticity [93], such as flow-solid interaction analysis of tube banks, has not appeared as yet. It is recommended that these two types of shell elements need to be further tested and developed for the present problem.

3) Many of the structural elements including both of the Ahmad element and the semiloop element are based on the eight-node serendipity element. Therefore, use of the serendipity element for flow calculations is recommended. The serendipity element or the complete quadratic element can approximate the curved and smooth boundary far better than linear elements.

4) Flow-solid interaction in a nest of thin cylinders subjected to cross-flows can be characterized by the large deformation of the structures which entails continuously changing flow domain. It would be advantageous, therefore, to use the Lagrangian formulation for the structural analysis and to use the Euler-Lagrangian formulation, introduced in Section 3.4, for the turbulent flow.

5) The body-fitted grid finite-difference method has already made significant progress toward flow-solid interaction analysis in tube banks. It is recommended that this method be further developed because it can be used together with the finite element structural analysis codes. The only drawback envisioned with this approach would be the complexities associated with a computer program structure originating from combining two numerical methods which are quite different in their nature.

6) Regardless of whether the finite element or the finite difference method is used for flow-solid interaction analysis in tube banks, difficulties may be encountered as a result of the use of unsteady turbulence models which are not well established as yet. There exist a few turbulence models well established for steady state turbulence models as has been discussed in Section 3.3. There also appeared a multiple scale k-ε turbulence model proposed by Hanjalic et al. [120] and an extended multiple scale turbulence model by Kim [12]. At this time, it is not clear which turbulence model would be most suitable to be extended to unsteady turbulent flows. It should be noted that the straight forward use of the standard k-ε turbulence model to unsteady flows has almost always been unsuccessful. Accordingly, any turbulence model to be used for flow-solid interaction needs to be tested against available experimental data. It is also recommended that tests for unsteady, turbulent flows be made of as many turbulence models as possible.

A successful numerical modeling of the flow-solid interaction would enhance the efficiency and confidence in the design of tube banks. For example, fretting of cylinders due to large deformation can be predicted directly, viscoplastic deformations which will shorten the lifetime of tube banks can be predicted directly, and any instability of tube banks subjected to cross-flows could be predicted using the nonlinear stability criterion analysis method [55].

REFERENCES

1. Blevins, R. D.: Flow Induced Vibrations. Van Nostrand Co., New York, 1977.

2. Chen, Y. N.: The Sensitive Tube Spacing Region of Tube Bank Heat Exchangers for Fluid-Elastic Coupling in Cross Flows. Presented at the Symposium on Fluid Structure Interaction Phenomena in Pressure Vessel and Piping System, ASME Winter Annual Meeting, Atlanta, Georgia, 1977.

3. Roberts, B. W.: Low Frequency Aeroelastic Vibrations in Cascade of Circular Cylinders. Mechanical Engineering Science Monograph No. 4, September 1966.

4. Connors, H. J.: Fluidelastic Vibration of Tube Arrays Excited by Cross Flow. Presented at the Symposium on Flow Induced Vibration in Heat Exchangers, ASME Winter Annual Meeting, December 1970.

5. Paidoussis, M. P.: Fluidelastic Vibration of Cylinder Arrays in Axial and Cross Flow. Proceedings of the Joint Pressure Vessels and Piping, Materials, Nuclear Engineering and Solar Conference, pp. 11-49, Denver, Colorado, June 1981.

6. Chen, Y. N.: Flow Induced Vibration and Noise in Tube Bank Heat Exchanges Due to von Karman Streets. ASME J. Engineering for Industry, Vol. 90, pp. 134-146, 1968.

7. Owen, P. R.: Buffeting Excitation of Boiler Tube Vibration. J. Mechanical Engineering Science, Vol. 7, pp. 431-439, 1965.

8. Paidoussis, M. P.: Flow Induced Vibrations in Nuclear Reactors and Heat Exchangers: Practical Experiences and State of Knowledge. Practical Experiences with Flow Induced Vibrations, pp. 1-81, Springer-Verlag, Berlin, 1980.

9. Crandal, S. H., and Mark, W. D.: Random Vibration in Mechanical Systems. Academic Press, New York, 1963.

10. Richard, E. J., and Mead, D. J.: Noise and Acoustic Fatigue in Aeronautics. J. Wiley and Sons, New Yorl, 1968.

11. Wambsganss, M. W., Jr., and Chen, S. S.: Tentative Design Guide for Calculating the Vibration Response of Flexible Cylindrical Elements in Axial Flow. Argonne National Laboratory Report ANL-ETD-71-07, 1971.

12. Chen, S. S., and Wambsganss, M. W., Jr.: Parallel Flow Induced Vibration of Fuel Rods. Nucl. Engr. Design, Vol. 18, pp. 253-278, 1972.

13. Ash, R. L.: Simulation of Turbulent Wall Pressure. NASA CR-2958, 1978.

14. Ash, R. L.: Simulation of Turbulent Wall Pressure. NASA CR-146534, 1976.

15. Wlezien, R. W., and Way, J. L.: Techniques for the Experimental Investigation of the Near Wake of a Circular Cylinder. J. AIAA, Vol. 17, No. 6, pp. 563-570, 1979.

16. Buckingham, A. C., Hall, M. S., and Chun, R. C.: Numerical Simulation of Compliant Material Response to Turbulent Flow. AIAA Paper AIAA-84-0537, January 1984.

17. Buckingham, A. C., Hall, M. S., and Chun, R. C.: Numerical Simulation of Compliant Material Response to Turbulent Flow. J. AIAA Vol. 23, No. 7, pp. 1046-1052, 1985.

18. Blevins, R. D.: Fluidelastic Whirling of a Tube Row. J. Pressure Vessel Technology, pp. 263-267, 1974.

19. Heinecke, E. P.: Fluidelastic Vibrations in Heat Exchangers with Tubes in Cross Flow. Proceedings of BNES International Conference on Vibration in Nuclear Plant, Keswick, May 1978.

20. Chen, S. S.: Guidelines for the Instability Flow Velocity of Tube Arrays in Crossflow. J. Sound and Vibration, Vol. 93, No. 3, pp. 439-445, 1984.

21. Chen, Y. N.: The Orbital Movement of and the Damping of the Fluidelastic Vibration of Tube Banks due to Vortex Formation, Part 2, Criterion for the Fluidelastic Orbital Vibration of Tube Arrays. Transactions of the ASME, Vol. 96, Series B, pp. 1065-1071, 1974.

22. Gross, H.: Investigations in Aeroelastic Vibration Mechanisms and Their Application in Design of Tubular Heat Exchangers. Ph.D. Thesis, Technical University of Hanover, 1975.

23. Gorman, D. J.: Experimental Development of Design Criteria to Limit Liquid Cross Flow Induced Vibration in Nuclear Reactor Heat Exchange Equipment. Nuclear Science and Engineering, Vol. 61, pp. 324-336, 1976.

24. Savkar, S. D.: A Brief Review of Flow Induced Vibration of Tube Arrays in Cross Flow. J. Fluid Engineering, Vol. 99, pp. 517-519, 1977.

25. Connors, H. J.: Fluidelastic Vibration of Heat Exchanger Tube Arrays. J. Mechanical Design, Vol. 100, pp. 347-353, 1977.

26. Pettigrew, M. J., Sylvestre, Y., and Campagna, A. O.: Vibration Analysis of Heat Exchanger and Steam Generator Designs. Nuclear Engineering and Design, Vol. 48, pp. 97-115, 1978.

27. Weaver, D. S. and Grover, L. K.: Cross Flow Induced Vibrations in a Tube Bank - Turbulent Buffeting and Fluidelastic Instability. J. Sound and Vibration, Vol. 59, pp. 277-294, 1978.

28. Chen, S. S., and Jendrzejczyk, J. A.: Experiments on Fluidelastic Instability in Tube Banks Subjected to Liquid Cross Flow. J. Sound and Vibration, Vol. 78, pp. 355-381, 1981.

29. Tanaka, H., Takahara, S., and Ohta, K.: Flow Induced Vibration of Tube Arrays with Various Pitch-to-Daimeter Ratios. ASME, Flow Induced Vibration of Circular Cylindrical Structures, Eds. Chen, S. S., et al., pp. 45-56, New York, 1982.

30. Paidoussis, M. P.: Fluidelastic Vibration of Cylinder Arrays in Axial and Cross Flow, State of the Art, ASME, Flow Induced Vibration Design Guidelines, Ed. Chen, P. Y., pp. 11-46, New York, 1980.

31. Blevins, R. D.: Discussions of Guidelines for the Instability Flow Velocity of Tube Arrays in Crossflow. J. Sound and Vibration, Vol. 97, No. 4, pp. 641-643, 1984.

32. Chen, S. S.: Author's Reply. J. Sound and Vibration, Vol. 97, No. 4, pp. 643-644, 1984.

33. Chen, S. S.: The Instability Flow Velocity of Tube Arrays in Cross Flow. Proceedings of the International Conference on Flow Induced Vibration in Fluid Engineering, Reading, England, September 1982.

34. Candel, S. M.: A Review of Numerical Methods in Acoustic Wave Analysis. ONERA TP No. 1983-83, 1983.

35. Bernhard, R. J.: A Finite Element Method for Synthesis of Acoustical Shapes. J. Sound and Vibration, Vol. 98, pp. 55-65, 1985.

36. Blevins, R. D.: Review of Sound Induced by Vortex Shedding from Cylinders. J. Sound and Vibration, Vol. 92, No. 4, pp. 415-520, 1984.

37. Quinn, M. C., and Howe, M. S.: The Influence of Mean Flow on the Acoustic Properties of a Tube Bank. Paper No. AIAA-84-2312, presented at the 9th AIAA/NASA Aeroacoustics Conference, Williamsburg, Virginia, October 1984.

38. Zdravkovich, M. M., and Nuttall, J. A.: On the Elimination of Aerodynamic Noise in a Staggered Tube Banks. J. Sound and Vibration, Vol. 34, No. 2, pp. 173-177, 1974.

39. Baird, R. C.: Pulsation Induced Vibration in Utility Steam Generation Units. Transactions of the ASME, Vol. 25, pp. 38-44, 1954.

40. Cohan, L. J., and Dean, W. J.: Elimination of Destructive, Self-excited Vibration in Large, Gas and Oil-Fired Utility Units. Chemical Process and Engineering, Vol. 87, pp. 223-228, 1965.

41. Morison, J. R.: The Force Exerted by Surface Waves on Piles. Petroleum Transactions, Vol. 189, pp. 149-157, 1950.

42. Srinivasan, R., and Mongia, H. C.: Numerical Computation of Swirling Recirculating Flow. NASA CR-165196, 1981.

43. Bankston, C. P., and Back, L. H.: Heat Transfer from Combustion Gases to a Single Row of Closely Spaced Tubes in a Swirl Crossflow Stirling Engine Heater. J. Heat Transfer, Vol. 104, pp. 55-61, 1982.

44. Singhal, A. K., et al.: Analysis of Physical-Chemical Processes Governing SSME Internal Fluid Flow. Cham of North America, Report No. 4045/22, Alabama, June 1985.

45. Chen, S. S.: A Mathematical Model for Cross Flow Induced Vibrations of Tube Rows. Technical Memorandum, ANL-CT-77-4, Argonne National Laboratory, Illinois, 1976.

46. Price, S. J., and Paidoussis, M. P.: An Improved Mathematical Model for the Stability of Cylinder Rows Subjected to Cross Flow. J. Sound and Vibration, Vol. 97, No. 4, pp. 615-640, 1984.

47. Price, S. J., and Paidoussis, M. P.: Fluidelastic Instability of a Double Row of Circular Cylinders Subjected to a Cross Flow. ASME J. of Design, Vibration, Acoustics, Stress and Reliability in Design, Vol. 105, pp. 59-66, 1983.

48. Simpson, A., and Flower, J. W.: An Improved Mathematical Model for the Aerodynamic Forces on Tandom Cylinders in Motion with Aeroelastic Applications. J. Sound and Vibration, Vol. 51, pp. 183-217, 1977.

49. Noh, W. F.: A Time-Dependent, Two-Space Dimensional, Coupled Eulerian-Lagrangian Code. Methods in Computational Physics, B. Alder, et al., Eds., Academic Press, New York, 1964.

50. Hirt, C. W., Amsden, A. A., and Cook, J. L.: An Arbitrary Lagrangian-Eulerian Computing Method for All Flow Speeds. J. Computational Physics, Vol. 14, pp. 227-253, 1974.

51. Donea, J., Giuliani, S., and Halleux, J. P.: An Arbitrary Lagrangian-Eulerian Finite Element Method for Transient Dynamic Fluid-Structure Interactions. Comput. Meths. Appl. Mech. Engrg., Vol. 33, pp. 689-723, 1982.

52. Belytschko, T., Flangan, D. P., and Kennedy, J. M.: Finite Element Methods with User-Controlled Meshes for Fluid-Structure Interactions. Comput. Meths. Appl. Mech. Engrg., Vol. 33, pp. 669-688, 1982.

53. Belytschko, T., Kennedy, J. M., and Schoeberle, D. F.: Quasi-Eulerian Finite Element Formulation for Fluid-Structure Interactions. Transactions of the ASME, J. Pressure Vessel Technology, Vol. 102, pp. 62-69, 1980.

54. Liu, W. K.: Development of Finite Element Procedures and Computer Implementation Aspects in Fluid-Structure Interactions. New Concepts in Finite Element Analysis. Eds. Hughes, et al., pp. 247-268, ASME, New York, 1981.

55. Zienkiewicz, O. C.: The Finite Element Method. 3rd Edition, McGraw-Hill, New York, 1977.

56. Halleux, J. P.: Modeling of Elasto-Plastic Material Behaviour. Report EUR-7329, Commissions of the European Communities, 1981.

57. Belytschko, T., and Hsieh, B. J.: Nonlinear Transient Finite Element Analysis with Convected Coordinates. Int. J. Num. Meth. Engr., Vol. 7, pp. 255-271, 1973.

58. Zienkiewicz, O. C., Loehner, R., Morgan, K., and Nakazawa, S.: Finite Elements in Fluid Mechanics - A Decade of Progress. Finite Elements in Fluids, Vol. 5, Eds. R. H. Gallagher, et al., pp. 1-26, J. Wiley and Sons, New York, 1984.

59. Oden, J. T.: RIP Methods for Stokesian Flow. Finite Elements in Fluids, Vol. 4, Eds. R. H. Gallagher, et al., pp. 305-318, J. Wiley and Sons, New York, 1982.

60. Hallquist, J. O.: User's Manual for DYNA-2D, An Explicit Two-Dimensional Hydrodynamics Finite Element Code with Interactive Rezoning. Report No. UCID-18756, Lawrence Livermore National Laboratory, 1982.

61. Hallquist, J. O.: User's Manual for DYNA3D and DYNAP (Nonlinear Dynamic Analysis of Solids in Three Dimensions). Report No. UCID-19156, Lawrence Livermore National Laboratory, 1981.

62. Hallquist, J. O.: Theoretical Manyal for DYNA3D. Report No. UCID-19401, Lawrence Livermore National Laboratory, 1983.

63. Orszag, S. A., and Kells, L. C.: Transition to Turbulence in Plane Poiseuille and Couette Flow. J. Fluid Mechanics, Vol. 96, pp. 159-205, 1980.

64. Orszag, S. A., and Patera, A. T.: Subcritical Transition to Turbulence in Plane Channel Flows. Physical Review Letters, Vol. 45, No. 12, pp. 989-993, 1980.

65. Cooley, J. W., and Tukey, J. W.: An Algorithm for the Machine Computation of Complex Fourier Series. Mathematics of Computation, Vol. 19, pp. 297-301, 1965.

66. Gottlieb, D., and Orszag, S. A.: Numerical Analysis of Spectral Method: Theory and Application. NSF-CMBS Monograph 26, SIAM, 1977.

67. Orszag, S. A.: Numerical Simulation of Incompressible Flow within Simple Boundaries, I. Galerkin (Spectral) Representations. Studies in Applied Mathematics, Vol. L., No. 4, 1971.

68. Orszag, S. A.: Comparison of Pseudospectral and Spectral Approximation. Studies in Applied Mathematics, Vol. LI, No. 3, 1972.

69. Nallasamy, M.: A Critical Evaluation of Various Turbulence Models as Applied to Internal Fluid Flow. NASA TP-2474, 1985.

70. Marvin, J. G.: Turbulence Modeling for Computational Aerodynamics. J. AIAA, Vol. 21, No. 7, pp. 941-955, 1983.

71. Lakshminarayana, B.: Turbulence Modeling for Complex Flows. Paper No. AIAA-85-1652, AIAA 18th Fluid Dynamics, Plasmadynamics, and Laser Conference, Cincinatti, Ohio, July 1985.

72. Launder, B. E., and Yang, W. M.: Secondary Flows in Ducts of Square Cross Section. J. Fluid Mechanics, Vol. 54, pp. 289-295, 1972.

73. Hanjalic, K., and Launder, B. E.: A Reynolds Stress Model of Turbulence and Its Application to Thin Shear Flows. J. Fluid Mechanics, Vol. 52, pp. 609-638, 1972.

74. Rodi, W.: A New Algebraic Relation for Calculating the Reynolds Stresses. EAMM, Vol. 56, pp. 219-221, 1976.

75. Launder, B. E., Reece, G. J., and Rodi, W.: Progress in the Development of a Reynolds Stress Turbulence Closure. J. Fluid Mechanics, Vol. 68, pp. 537-566, 1975.

76. Rodi, W.: Examples of Turbulence Models for Incompressible Flows. J. AIAA, Vol. 20, No. 7, pp. 872-879, 1982.

77. Hanjalic, K., and Launder, B. E.: Contribution Towards a Reynolds Stress Closure for Low Reynolds Number Turbulence. J. Fluid Engineering, Vol. 74, pp. 593-610, 1976.

78. Launder, B. E., and Spalding, D. B.: The Numerical Computation of Turbulent Flow. Comp. Meth. Appl. Mech. Engrg., Vol. 3, pp. 269-289, 1974.

79. Patel, V. C., Rodi, W., and Scheuerer, G.: Turbulence Models for Near-Wall and Low Reynolds Number Flows: A Review. J. AIAA, Vol. 23, No. 9, pp. 1308-1319, 1985.

80. Jones, W. P., and Launder, B. E.: The Prediction of Laminarization with a Two-Equation Model of Turbulence. Int. J. Heat Mass Transfer, Vol. 5, pp. 301-314, 1973.

81. Naot, D., and Rodi, W.: Numerical Simulation of Secondary Currents in Open Channel Flow with an Algebraic Stress Turbulence Model. ASCE J. Hydraulic Div., Vol. 108, pp. 948-969, 1982.

82. Gibson, M. M.: Prediction of Curved Free Shear Layers with a Reynolds Stress Model of Turbulence. Proc. the 2nd Symposium on Turbulent Shear Flows, London, 1979.

83. Celik, I., and Rodi, W.: Calculation of Oscillatory Turbulent Flows in Open Channels. Proc. Energy Sources Technology Conference, New Orleans, Louisiana, February, 1984.

84. Telionis, D. P.: Unsteady Viscous Flows. Springer-Verlag, New York, 1981.

85. Boyle, D. K., and Golay, M. W.: Measurement of a Recirculating Two-Dimensional Turbulent Flow and Comparison to Turbulence Model Predictions. II. Transient Case. ASME Winter Annual Meeting, Boston, MA., November 1983.

86. Schumann, U., Grotzback, G., and Kleiser, L.: Direct Numerical Simulation of Turbulence. Prediction Methods for Turbulent Flows, Ed. W. Kollmann, Hemisphere Publishing Co., New York, 1980.

87. Leonard, A.: Energy Cascade in Large Eddy Simulations of Turbulent Fluid Flows. Advances in Geophysics, Vol. 18A, pp. 237-248, 1974.

88. Deardroff, J. W.: A Numerical Study of Three-Dimensional Turbulent Channel Flow at Large Reynolds Number. J. Fluid Mechanics, Vol. 41, pp. 453-480, 1970.

89. Lilly, D. K.: Proceedings IBM Scientific Computing Symposium on Environmental Sciences, IBM Form No. 320-1951, 1967.

90. Patankar, S. V.: Numerical Heat Transfer and Fluid Flow. Hemisphere Publishing Co., 1980.

91. Schumann, U.: Subgrid Scale Model for Finite Difference Simulations of Turbulent Flows in Plane Channels and Annuli. J. Computational Physics, Vol. 18, pp. 376-404, 1975.

92. Moin, P., and Kim, J.: Numerical Investigation of Turbulent Channel Flow. J. Fluid Mechanics, Vol. 118, pp. 341-377, 1982.

93. Hughes, T. J. R., and Taylor, R. L.: Unconditionally Stable Algorithms for Quasi Static Elasto-Viscoplastic Finite Element Analysis. Computers and Structures, Vol. 8, pp. 169-173, 1978.

94. Owen, D. R. J., and Hinton, E.: Finite Elements in Plasticity. Pineridge Press Ltd., Swansea, U. K., 1980.

95. Perzyna, E.: Fundamental Problems in Viscoplasticity. Recent Advances in Applied Mechanics, Academic Press, New York, 1966.

96. Dawson, P. R.: Development of Models for Simulating Warm and Hot Forming Processes. Proc. Manufacturing Systems Research Conference, SME, 1985.

97. Anand, L.: Constitutive Equations for the Rate Dependent Deformaiton of Metals at Elevated Temperatures. ASME, J. Engineering Materials and Technology, Vol. 104, pp. 12-17, 1982.

98. Bodner, S. R., and Partom, Y.: Constitutive Equations for Elastic-Viscoplastic Strain Hardening Materials. ASME, J. Applied Mechanics, Vol. 42, pp. 385-389, 1975.

99. Rodal, J. J. A., Steigmann, D. J., and Witmer, E. A.: Numerical Simulation of Transient Finite Deformations of Thin Beams. J. Applied Mechanics, Vol. 50, pp. 765-769, 1983.

100. Rodal, J. J. A., and Witmer, E. A.: Finite Strain Large Deflection Elastic-Viscoplastic Finite Element Transient Response Analysis of Structures. NASA CR-159874, 1979.

101. Bathe, K. J., and Wilson, E. J.: Numerical Methods in Finite Element Analysis. Prentice-Hall, New Jersey, 1976.

102. Schreyer, H. L., Kulak, R. F., and Kramer, J. M.: Accurate Numerical Solutions for Elastic-Plastic Models. ASME, J. Pressure Vessel Technology, Vol. 101, No. 3, pp. 226-234, 1979.

103. Wambsganss, M. W., Yang, C. I., and Halle, H.: Fluidelastic Instability in Shell and Tube Heat Exchangers − A Framework for a Prediction Method. Proc. ASME Winter Annual Meeting, New Orleans, December 1984.

104. Sha, W. T., Yang, C. I., Kao, T. T., and Cho, S. M.: Multidimensional Numerical Modeling of Heat Exchangers. ASME, J. Heat Transfer, Vol. 104, pp. 417-425, 1982.

105. Zienkiewicz, O. C., Loehner, R., Morgan, K., and Nakazawa, S.: Finite Elements in Fluid Mechanics - A Decade of Progress. Finite Elements in Fluids, Vol. 5, J. Wiley and Sons, New York, 1984.

106. Kwak, D., and Chang, J. L. C.: A Three Dimensional Incompressible Navier-Stokes Flow Solver, Part I. - INS3D Code. CFD Workshop, University of Tennessee Space Institute, Tullahoma, Tennesses, June 1985.

107. Chang, J. L. C., and Kwak, D.: A Three Dimensional Incompressible Navier-Stokes Solver, Part II. - Space Shuttle Main Engine (SSME) Power Head Simulation. CFD Workshop, University of Tennessee Space Institute, Tullahoma, Tennessee, June 1985.

108. Rogers, S. E., Kaul, U. K., and Kwak, D.: A Numerical Study of Single and Multiple LOX Posts and Its Application to the Space Shuttle Main Engine (SSME). Proceedings AIAA Aerospace Science Meeting, Reno, Nevada, January 1986.

109. Brooks, A. N., and Hughes, T. J. R.: Streamline Upwind/Petrov-Galerkin Formulations for Convection Dominated Flows with Particular Emphasis on the Incompressible Navier-Stokes Equation. Comput. Meth. Applied Mech. Engrg., Vol. 32, pp. 199-259.

110. Zienkiewicz, O. C.: Flow Formulation for Numerical Solution of Forming Processes. Numerical Analysis of Forming Processes, Eds. J. F. T. Pittman, et al., J. Wiley and Sons, New York, 1984.

111. Taylor, C., and Hughes, T. G.: Finite Element Programming of the Navier-Stokes Equation. Pineridge Press, Swansea, U. K., 1980.

112. Donea, J.: A Taylor-Galerkin Method for Convective Transport Problems. Int. J. Nume. Meth. Engrg., Vol. 20, pp. 101-119, 1984.

113. Lohner, R., Morgan, K., and Zienkiewicz, O. C.: The Solution of Nonlinear Hyperbolic Equation Systems by the Finite Element Method. Int. J. Nume. Meth. Engrg., Vol. 4, pp. 1043-1063, 1984.

114. Donea, J., Giuliani, S., Laval, H., and Quartapelle, L.: Time-Accurate Solution of Advection-Diffusion Problems by Finite Elements. Comp. Meth. Applied Mech. Engrg., Vol. 45, pp. 123-145, 1984.

115. Yu, C. C., and Heinrich, J. C.: Petrov-Galerkin Methods for the Time Dependent Convective Transport Equation. will appear in Int. J. Nume. Meth. Engrg., 1986.

116. Balija, B. R., and Patankar, S. V.: A New Finite Element Formulation on Convection-Diffusion Problems. Numerical Heat Transfer, Vol. 3, pp. 393-409, 1980.

117. Prakash, C., and Patankar, S. V.: A Control Volume Based Finite Element Method for Solving the Navier-Stokes Equations Using Equal-Order Velocity-Pressure Interpolation. Numerical Heat Transfer, Vol. 8, pp. 259-280, 1985.

118. Prakash, C.: An Improved Control Volume Finite Element Method for Heat and Mass Transfer and for Fluid Flow Using Equal-Order Velocity-Pressure Interpolation. Numerical Heat Transfer, in press, 1986.

119. Kikuchi, N., Oden, J. T., and Song, Y. J.: Convergence of Modified Penalty Methods and Smoothing Schemes of Pressure for Stokes' Flow Problems. Finite Elements in Fluids, Vol. 5, Eds. R. H. Gallagher, et al., pp. 107-126, J. Wiley and Sons, New York, 1984.

120. Hanjalic, K., Launder, B. E., and Schiestel, R.: Multiple-Time-Scale Concepts in Turbulent Transport Modeling. In Turbulent Shear Flows, Vol. 2, Eds. L. J. S. Bradbury, et al., Springer-Verlag, pp. 36-49, 1980.

121. Kim, S.-W.: Finite Element Computation of Turbulent Flows and an Extended Multiple-Scale Turbulence Closure Model. In preparation.

122. Taylor, C., Thomas, C. E., and Morgan, K.: F. E. M. and the Two Equation Model of Turbulence. Proc. the 2nd Int. Conf. on Numerical Methods in Laminar and Turbulent Flow, Eds. C. Taylor and B. A. Schrefler, Venice, Pineridge Press, 1981.

123. Smith, R. M.: On the Finite Element Calculation of Turbulent Flow Using the k-ε Model. Int. J. Nume. Fluids, Vol. 4, pp. 303-319, 1984.

124. Benim, A. C., and Zinser, W.: Investigation into the Finite Element Analysis of Confined Turbulent Flows Using a k-ε Model of Turbulence. Comput. Meth. Appl. Mech. Engrg., Vol. 51, pp. 507-523, 1985.

125. Atkins, D. J., Maskell, S. J., and Patrick, M. A.: Numerical Prediction of Separated Flows. Int. J. Nume. Meth. Engrg., Vol. 15, No. 1, pp. 129-144, 1980.

126. Irons, B., and Ahmad, S.: Techniques of Finite Elements. J. Wiley and Sons, New Yorl, 1980.

127. Brebbia, C. A., and Walker, S.: Boundary Element Techniques in Engineering, Newnes-Butterworths, London, 1980.

APPROVAL

A CRITICAL EVALUATION OF VARIOUS METHODS FOR THE
ANALYSIS OF FLOW-SOLID INTERACTION IN A NEST OF
THIN CYLINDERS SUBJECTED TO CROSS FLOWS

By Sang-Wook Kim

The information in this report has been reviewed for technical content. Review of any information concerning Department of Defense or nuclear energy activities or programs has been made by the MSFC Security Classification Officer. This report, in its entirety, has been determined to be unclassified.

G. F. McDonough
Director, Systems Dynamics Laboratory

1. REPORT NO. NASA CR - 178996	2. GOVERNMENT ACCESSION NO.	3. RECIPIENT'S CATALOG NO.

4. TITLE AND SUBTITLE	5. REPORT DATE
A Critical Evaluation of Various Methods for the Analysis of Flow-Solid Interaction in a Nest of Thin Cylinders Subjected to Cross Flows	January 1987
	6. PERFORMING ORGANIZATION CODE

7. AUTHOR(S) Sang-Wook Kim *	8. PERFORMING ORGANIZATION REPORT #

9. PERFORMING ORGANIZATION NAME AND ADDRESS	10. WORK UNIT, NO.
George C. Marshall Space Flight Center Marshall Space Flight Center, Alabama 35812	11. CONTRACT OR GRANT NO. NAS8-35918
	13. TYPE OF REPORT & PERIOD COVERED

12. SPONSORING AGENCY NAME AND ADDRESS	
National Aeronautics and Space Administration Washington, D.C. 20546	Contractor Report
	14. SPONSORING AGENCY CODE

15. SUPPLEMENTARY NOTES   Prepared by Atmospheric Sciences Division, Systems Dynamics Laboratory, Science and Engineering Directorate.

* Universities Space Research Association.

16. ABSTRACT

The report presents a review of various experimental, analytical, and numerical analysis methods for flow-solid interaction of a nest of cylinders subjected to cross-flows.

A nest of cylinders subjected to cross-flows can be found in numerous engineering applications including the Space Shuttle Main Engine - Main Injector Assembly (SSME-MIA) and nuclear reactor heat exchangers. Despite its extreme importance in engineering applications, understanding of the flow-solid interaction process is quite limited and design of the tube banks are mostly dependent on experiments and/or experimental correlation equations.

For future development of major numerical analysis methods for the flow-solid interaction of a nest of cylinders subjected to cross flow, various turbulence models, numerical analysis methods for flows, the finite element computational method of nonlinear structural dynamics, and existing laminar flow-solid interaction analysis methods are included in this report.

17. KEY WORDS	18. DISTRIBUTION STATEMENT
Flow-Solid Interaction, Finite Element Method, Finite Difference Method, Turbulent Flow, Elasto-Viscoplasticity, Cross-Flow, Tube Bank	Unclassified — Unlimited

19. SECURITY CLASSIF. (of this report)	20. SECURITY CLASSIF. (of this page)	21. NO. OF PAGES	22. PRICE
Unclassified	Unclassified	74	NTIS